Appendix D

Potential Field Data – Magnetic Surveys

Introduction

Potential field (gravity and magnetic) data available at the time of the original LTSP, (e.g. McCulloch and Chapman, 1977; Beyer and McCulloch, 1988; Chapman et al., 1989) had insufficient resolution for detailed characterization of the Hosgri fault zone. Residual magnetic intensity data offshore DCPP, presented in LTSP Plate Q43m-2 (PG&E, 1989a), were flown in 1976 with a flight line spacing of 1 mile (1.6 km) at an altitude of 2000 feet (610m) above sea level. Their primary utility was in the identification of changes in basement rock characteristics and morphology and in confirming seismic data interpretation of basement structures.

Modern high resolution geophysical data have significantly improved the imaging of basement structure. In 2008 and 2009 new marine magnetic and aeromagnetic data were collected in the study area. Aeromagnetic data were collected at a lower altitude (305 m v. 610 m) with half of the line spacing (800 m v 1.6 km) using differential GPS navigation. Marine magnetic data were collected at 400 m line spacing. Additional aeromagnetic data at ~ 50 m elevation and 150 m line spacing were collected along the coastline between Pt. Buchon and Pt. San Luis in late 2009. Figure D-1 compares the earlier LTSP magnetic data with the high resolution data that was collected in 2009.

Aeromagnetic Data

Total-field aeromagnetic data were collected by Eon Geosciences, Inc. from July to September 2008 along the central California Coast Ranges from north of Cape San Martin, near San Simeon, to Point Concepcion. A total of 20,508 line-kilometers of data were collected using a Geometrics G-822A cesium-vapor magnetometer along flight lines spaced 800 m apart at a nominal terrain clearance of 305 meters. Tie lines were flown 8,000 m apart. Figure D- 2 shows the survey area. Two areas within the survey area were not flown because of proximity to condor nesting sites. Aeromagnetic data were collected at a 10 Hz sampling rate, and were adjusted for tail sensor lag and diurnal field variations. Further data processing included micro leveling using the tie lines and subtraction of the reference field defined by IGRF2005 extrapolated to August 1, 2008. Data were transformed to a Universal Transverse Mercator Projection (Base Latitude 0°, Central Meridian -123° W.) and interpolated to a square grid with a grid interval of 200 m using the principle of minimum curvature (Briggs, 1974). A magnetic base station was established near the San Luis Obispo Airport. Base station readings were recorded every second using a GEM Systems Overhauser GSM-19 magnetometer. A contour map of the aeromagnetic data was published as USGS Open File Report 2009- 1044 (Langenheim et al., 2009a) and is shown in Figure D-3.

An additional 933 line-kilometers of total field aeromagnetic data were collected by New-Sense Geophysics in October 2009 between Pt. Buchon and Pt. San Luis using a Scintrex CS-3 Cesium vapor magnetometer mounted on Bell 206 B3 helicopter with a fixed stinger assembly (New Sense Geophysics, 2010). A three-axis Bartington fluxgate magnetometer was used to measure the orientation and rates of change of the aircraft to compensate for magnetic fields generated by the aircraft itself. Flight lines were spaced 150 m apart at a nominal terrain clearance of 50 to 100 m. Tie lines were flown 1500 m apart. These data were collected by helicopter to fill the gap between the marine and

fixed wing surveys along the coastal zone to provide higher resolution of features near the shoreline. Figure D-4 shows the area of the 2009 survey and the corrected Total Magnetic Intensity map for the survey area. The sampling rate for the cesium and fluxgate magnetometers and radar altimeter was at 10 Hz. Data processing included micro leveling using the tie lines and subtraction of the reference field defined by IGRF2005. A magnetic base station was established at DCPP in an area of low magnetic gradient free from cultural electrical and magnetic noise sources (Latitude 35.211513, Longitude -120.845162). Base station readings were recorded every second using an Overhauser GSM-19 magnetometer.

Marine Magnetic Data

Marine magnetic data were collected by the USGS in 2008 and 2009 (Sliter et al., 2009, revised 2010) using a Geometrics G882 cesium-vapor magnetometer that was towed approximately 30 m behind the research vessel *R/V Parke Snavely* in 2008 and approximately 50 m behind the vessel in 2009. Magnetic data were collected at a 10-Hz sampling rate on a line spacing of 800 m along shore-perpendicular transects simultaneously with the mini sparker seismic-reflection data (see Appendix H). Additional magnetic transects were run across segments of the Hosgri Fault Zone in 2008, resulting in a localized line spacing of 400 m. In 2009, an additional series of marine magnetics transects were conducted closer to shore between Pt. Buchon and Pt. San Luis, resulting in a uniform line spacing of 400 m for the survey area. Seismic-reflection and marine magnetic data were also collected along three shore-parallel tie lines. See Figure D-5 for survey area. A magnetic base station was set up onshore in Morro Bay State Park on the south flank of Black Hill (Lat 35.3536° N., Long 120.8314° W.) in 2008 to continuously measure the local magnetic field in order to remove diurnal field variations from the offshore survey. In 2009, two base stations were established onshore during different portions of the survey, one in Morro Bay State Park and one near Avila beach in Wild Cherry Canyon (Lat 35.1870° N, Long 120.7467° W). See Figure D-6 for base station locations. Base-station readings were recorded every minute, using a Geometrics G856 proton-precession magnetometer.

Initial processing of the magnetic data involved smoothing, mainly to remove noise from the mini sparker source. The smoothed data resulted in approximate along-track data spacing of 10 m for lines where seismic-reflection data were also collected (boat speed, 4 knots), and 25 m along the magnetometer-only lines (boat speed, 10 knots). Further processing included removal of the diurnal field variation by using the magnetic-base-station readings and subtracting the reference field defined by the IGRF2005. Data were imported into the Geosoft Oasis montaj™ geophysical software package, where survey lines were leveled by using the tie lines and then gridded at 200 m (Figure D-6). Marine magnetic data were subtracted from the fixed wing aeromagnetic data (Langenheim et al., 2009a) to produce a residual magnetic anomaly map dominated by magnetic sources in the shallow subsurface (< 500m below the seafloor (see Figure D-7)). Figure D-8 shows the merged onshore and offshore magnetic data. The marine data were filtered to effectively place those data at the same height as the regional aeromagnetic survey (Langenheim et al., 2009b). Figures D-7 and D-8 both show the dominant NW

magnetic grain that is truncated by the Hosgri fault zone on the west and bounded by the Oceanic fault on the east.

2D Processing of Magnetic Field Data

The magnetic intensity data from the helicopter survey were processed by Fugro Magnetic and Gravity Surveys, Inc. (Houston, Texas) with assistance from FWLA to aid in the interpretation of shallow magnetic features along the Shoreline fault zone (Fugro Gravity and Magnetics Services, 2010) . Since the magnetic inclination in this area is approximately 59º, the total magnetic intensity anomaly field has anomalies that are not symmetrical and generally not centered over the causative magnetic source bodies or contacts between bodies of different magnetic susceptibilities. However, the inclination of 59º is considered to be fairly high latitude and therefore the total magnetic intensity anomalies for simple tabular shaped sources will be dipolar but with a larger positive peak than negative trough. This also means the differences in line azimuth in 2D modeling will not be as important as for low magnetic latitudes and inclinations. The objectives of the processing included positioning anomalies over their sources using reduction to pole (RTP) (Li, 2008) and highlighting lateral boundaries using tilt angle and horizontal gradients (Miller and Singh, 1994; Verduzco et al., 2004). To facilitate calculation of these derivative magnetic anomaly maps, the helicopter – total magnetic intensity anomaly data (Figure D-4) were re-gridded with a 30 m cell size (Figure D-9). The 30-m cell size is about one fifth the line spacing and about as small as recommended.

The first processing step was the reduction-to-pole (RTP) transformation of the re-gridded data, which removes first-order magnetic field inclination effects to better position anomalies over their sources (Figure D-10). Reduction to the pole makes the simplifying assumption that the rocks in the survey area are all magnetized parallel to Earth's magnetic field. This is true in the case of rocks with an induced magnetization only, however remnant magnetization will not be correctly dealt with if the remnant direction is different to the direction of Earth's magnetic field. Thus the RTP transformation is associated with varying degrees of error and introduction of noise, such that only first-order features are robust. The primary change is that many of the RTP magnetic anomalies (Figure D-10) are narrower than the TMI anomalies (Figure D-9) and sometimes the position of peak anomaly amplitudes have shifted slightly compared to the total magnetic intensity anomalies.

There are factor of 10 differences in water depth within the span of the helicopter magnetic survey. The helicopter data acquisition elevation was small (50 m) relative to water depths that range from 10 m near the coast to over 100 m in the southwestern end of the helicopter survey area (Figure D-11). Thus, it is important to consider the effects of bathymetry on the amplitude and width of the RTP magnetic anomalies and derivative maps. Figure D-11 superimposes bathymetry contours on the RTP magnetic field map. The Shoreline fault RTP anomaly is very narrow in the shallow (~10 m) water nearest to shore, but the peak anomaly amplitude decreases and the anomaly width increases by about a factor of three in 40 m of water (Figure D-11). All the large-amplitude offshore RTP anomalies decrease in amplitude and broaden to the west as they trend toward water depths > 40 m (Figure D-11) consistent with first-order effects water depth being on the

order of the helicopter flight elevation of 50 m. Calculations using a first-order vertical dipole approximation indicate that for the flight elevation of 50 m, RTP anomalies observed in 40 m of water should have widths about three times wider and amplitudes about 40% of RTP anomalies in areas with 10 m water depths. Hence, while the peaks of the RTP anomalies are useful to provide first-order estimates of the position of source bodies, the widths and amplitudes of the RTP anomalies as they trend toward deeper water should not be inferred to mean that the tops of source bodies are moving significantly below the seafloor, are becoming broader, or are necessarily starting to dip significantly away from vertical.

The RTP image was used to calculate vertical and horizontal gradients to produce a tilt angle anomaly map based on the arc tangent of the vertical-to-horizontal gradient ratio (Figure D-12). The tilt angle highlights the lateral extent of magnetic source bodies. From Miller and Singh (1994), "The tilt angle may be used to detect the presence of sources of potential field anomalies and to provide information about their horizontal extent. It has the attractive property of being positive over the source, crosses through zero at, or near, the edge of a vertical sided source, and it is negative outside the source region. The tilt angle has the additional attribute, unique among the various potential field edge detectors, of responding equally as well to shallow and to deep sources and is, therefore, able to resolve the presence of subtle deeper sources which are often swamped in the larger responses of shallower sources." While these attributes of tilt-angle are generally true for level ground, the abrupt change in the seafloor elevations and slopes between the north and south sides of the Shoreline fault and the N40W fault have different effects on the vertical versus horizontal components of RTP total magnetic intensity. In particular, the bathymetry contours intersect the western Shoreline and N40W fault segments at shallow angles (Figure D-11). Most of the Shoreline fault closely follows a series of narrow prominent tilt-angle anomalies near the shore (Figure D-12). However, the tilt-angle anomaly along the southwestern portions of the Shoreline and N40W faults may in part be smeared out laterally to the southwest (compare Figure D-11 and D-12) due to quite different water depth characteristics across the deeper water portions of these faults.

The horizontal gradient of RTP results in positive peaks along the edges of blocks. However, for thin steeply dipping sources a double positive anomaly results. The horizontal gradient results are important because the consistent double positive peaks along all the Shoreline fault segments where water depth is less than 40 m indicate that these portions of the source body along the Shoreline fault are near-vertical (Figure D-13). As the water depth becomes about 40 m or more, the horizontal gradient becomes more diffuse and lower amplitude (Figure D-13). The greater distance from the flight elevation of 50 m to the top of the source bodies as water depth increases broadens the horizontal anomaly and reduces its amplitude, resulting in a lower amplitude, broader horizontal gradient in the deeper water portions of Figure D-13. This result confirms that the apparent broadening of the tilt-angle anomalies in regions with water depths > 40 m (Figure D-14) is at least in part an artifact of the increased water depth. Thus, both the horizontal gradient (Figure D-13) and narrow tilt-angle anomaly regions in water shallower than 40 m (Figure D-14) suggest a source body that has a steep dip and is on

the order of 200 m thick or less. There is a one-to-one spatial correlation of the position of the double positive peaks of horizontal gradient with the narrow tilt-angle anomalies (Figure D-14) and a first-order one-to-one spatial correlation of the tilt-angle anomalies with the Shoreline fault segments (Figure D-15).

The RTP, horizontal gradient, and tilt-angle maps are all consistent with a near-vertical source body associated with the Shoreline fault along all the near-shore segments of the fault (Figures D-10, D-14, and D-15). The possible dips for the source bodies along portions of the Shoreline and N40W faults located in regions with water depths of 40 m or more are not as well constrained due to possible effects of deep water relative to the helicopter flight elevation of 50 m. However, even in the regions with water depths of 40-50 m, the horizontal gradient map shows double positive peak anomalies along the Shoreline and N40W faults (Figure D-13), suggesting that the deeper water portions of these faults are steeply dipping. 2D modeling described below is used to further investigate magnetic constraints on Shoreline fault dip.

2D Modeling of Magnetic Anomaly Data

2D forward modeling of the magnetic anomaly data is used to evaluate alternative magnetic models to determine the first-order magnetic anomaly constraints on fault dips and magnetic basement depth. Modeling of the magnetic-intensity data from the combined marine, fixed wing, and high-resolution helicopter surveys were evaluated by Fugro Magnetic and Gravity Services (Houston, Texas) and Fugro William Lettis & Associates to aid in the interpretation of prominent magnetic features. A single profile location was selected to incorporate the maximum amount of geologic and geophysical constraints available in the area while crossing the Hosgri and Shoreline faults and the central portion of the Irish Hills. Geologic mapping constrains surface geology and formation dips along the profile. Constraints on the structure of the Pismo syncline and Tertiary sediments are provided by proprietary seismic reflection profiles in the central Irish Hills. These seismic reflection profiles and the Honolulu-Tidewater well located in the central Irish Hills (PG&E, 1989b) provide constraints on the structure of the Pismo syncline at depth, including the minimum possible thickness of Tertiary sediments within the syncline along the 2D magnetic anomaly profile. The position of the profile was adjusted to incorporate the highest concentration of gravity measurements in the offshore and onshore sections of the profile.

The helicopter magnetic data being flown at lower elevation of 50 m than the aeromagnetic data (305 m) provide better resolution of shallow magnetic anomalies than the aeromagnetic data. Therefore, the higher resolution helicopter magnetic data was spliced-in into the portions of the profile where it was available for use in the 2D modeling. Total Magnetic Intensity (TMI) values were used for the modeling of the helicopter magnetic data and Residual Magnetic Intensity (RMI) values were used by Langenheim et al. (2009b) to model the marine and fixed wing magnetic data. As a result, there is a “DC” shift of 47,847 nT between these two data sets (TMI-IGRF).

The magnetic profile modeling is simplified if a single azimuth profile is compatible with modeling faults with disparate strike (Hosgri, Shoreline, and Los Osos faults). To determine if this was feasible a test model was built in order to determine the effect of a change in line azimuth from 008º to 058º (clockwise rotation relative to north). The trial magnetic model includes a dyke-like feature or magnetization along a fault plane, and a lateral contact between strongly magnetized and non-magnetic basement (Figure D-16). The difference between the 008º azimuth magnetic anomaly (Figure D-16) and the 058º azimuth model (Figure D-17) is significant in terms of absolute amplitude but the relative responses are similar. Therefore, a single strike for the entire line profile was deemed acceptable for 2D magnetic modeling.

A new geological cross section was compiled by FWLA for 2D model profile 1. The cross section was geo-referenced and digitized using FGMS 2D modeling software. The digitized cross section elements were then transformed into polygons for the initial model. Magnetic depth to basement analyses were performed for the vicinity of the 2D model Line 1 only using FGMS Magprobe™ software (Li, 2003). FWLA confirmed that magnetic basement in this area may be ophiolite or melange, and perhaps not that of typical granitic or metamorphic composition. A total of 31 forward models were evaluated and successively modified to produce a model that provided a reasonable fit to the magnetic and gravity anomaly data along 2D model profile 1 that was consistent with available geologic and geophysical data, including first-order basement depth estimates in the offshore region (Figure D-18). Depth-to-basement estimates in the onshore region may be biased by shallow source bodies and complex shallow structure, along the south side of the Pismo syncline, so the onshore depth-to-basement estimates were not used as constraints in this part of the section (Figure D-18).

In forward model 31, the narrow anomaly just offshore that coincides with the mapped position of the Shoreline fault is reproduced using a steeply-dipping shallow source body (Figure D-18). To determine if other source body configurations could fit the magnetic anomaly profile equally well as series of alternative forward models were constructed that focused on the region near the Shoreline fault shown in forward model 31 (Figure D-18). Forward model 33 evaluated a thin, vertical source body that extended nearly to basement (Figure D-19). The calculated magnetic anomaly does not fit as well due to the shorter predicted wavelength than observed near the Shoreline fault (Figure D-19). Forward model 34 used a thicker, 200-m wide vertical source body that produced a much better fit near the Shoreline fault (Figure D-20). A north-dipping source body near the Shoreline fault in forward model 35 produces a much poorer fit to the magnetic anomaly data, particularly on the south side of the fault and the source body has to be shifted south of the Shoreline fault to match the position of the peak anomaly amplitude (Figure D-21). The south-dipping source body in forward model 36 produces an excellent fit to the magnetic anomaly, but requires moving the top of the source body 200 m north of the Shoreline fault (Figure D-22). Thus, only a near-vertical Shoreline fault source body configuration that is consistent with both 2D modeling profile 1 (Figures D-18 and D-20a and b), the RTP map (Figure D-10), the horizontal gradient map (Figure D-13), and the tilt-angle map (Figure D-15). Significant north or south dips requiring displacement the top of the source body several hundred meters from the mapped trace of the Shoreline

fault (Figures D-21 and AD-22). The 2D profile modeling shows that the source body along the Shoreline fault need not extend more than 200-300 m below the surface (Figure D-18), but can extend to at least 4 km and fit the magnetic anomaly data equally well (Figure D-20a and b). Thus, the magnetic data indicate that the source body associated with the Shoreline fault is most likely to be nearly vertical, with a width on the order of 200 m, and extends from near-surface to a depth of several hundred meters to several km below the surface.

References

Beyer, L.A. and McCulloch, D.S., 1988, Free-air gravity anomaly map of the offshore Santa Maria Basin, *U.S. Geol. Surv. Open-File Rep* 89-322 1 map, scale 1: 125,000

Briggs, I.C., 1974, Machine contouring using minimum curvature: *Geophysics*, **39**, 39-48.

Chapman, R.H., Beyer, L.A., and Youngs, L.G., 1989, Bouguer gravity and magnetic anomaly map of the south-central California Continental margin (Map 4c) , in Greene H.G. and Kennedy, M.P., eds., California Continental Margin Geologic Map Series: South-Central California continental margin- Area 4 of 7, California Division of Mines and Geology, Scale 1:250,000

Fugro Gravity and Magnetics Services, 2010, PG&E California Gravity and Magnetic Data Modeling, Interpretation Interim Report, 53 pp.

Langenheim, V.E., Jachens, R.C, and Moussaoui, K., 2009a, Aeromagnetic Survey Map of the Central California Coast Ranges, USGS Open File Report 2009-1044 http://pubs.usgs.gov/of/2009/1044/

Langenheim, V.E., Jachens, R.C., Graymer, R.W. and Wentworth, C.M., 2009b, Constraints on 3-Dimensional structure of the central California Coast Ranges from gravity and magnetic data (abs), *Seism. Res. Lett.*, **80**, 323

Li, X., 2003, On the use of different methods for estimating magnetic depth: The Leading Edge, v. 22, no. 11, p. 1090-1099

Li, X., 2008, Magnetic reduction-to-the-pole at low latitudes: observations and considerations, Practical considerations: The Leading Edge, v. , no. , 990-1002

McCulloch, D.S. and Chapman, R.H., 1977, Maps showing residual magnetic intensity along the California coast, Lat. 37° 30’N to 34° 30’N, US Geological Survey Open File Rpt. 77-79, 14 aeromagnetic maps, scale 1:250,000

Miller, H. G., and V. Singh, 1994, Potential field tilt - a new concept for location of potential field sources: Journal of Applied Geophysics, v. 32, p. 213–217.

New Sense Geophysics, 2010, Point Buchon: Helicopter aeromagnetic geophysical survey for Pacific Gas and Electric Company, December 2nd – December 5th, 2009. PG&E No. 2500257867, NSG No. HM191015, Toronto, Canada, 40 p.

Pacific Gas and Electric Company (PG&E), 1989a, Response to question Q43m-2, in Response to questions 43k, 43l, 43m, 43n, 43o, and 43p, Gravity and magnetic contour maps, U.S. Nuclear Regulatory Commission Document No. 50-275 and No. 50-323, January 1989.

Pacific Gas and Electric Company (PG&E), 1989b, Response to question Q43m-2, in Response to questions 43r, 43s, 43t, 43u, 43v, and 43w, Drill logs and core descriptions Honolulu Tidewater USL Heller Lease well, U.S. Nuclear Regulatory Commission Document No. 50-275 and No. 50-323, January 1989.

Sliter, R.W., Triezenberg, P.J., Hart, P.E., Watt, J.T., Johnson, S.Y., and Scheirer, D.S., 2009, revised 2010. High-resolution seismic reflection and marine magnetic data along the Hosgri Fault Zone, Central California, USGS Open File Report 2009-1100, version 1.1 http://pubs.usgs.gov/of/2009/1100 /

Verduzco, B., J. D. Fairhead, C. M. Green, C. Mackenzie, 2004, New insights into magnetic derivatives for structural mapping: The Leading Edge, v. 23, no. 2, p. 116-119.

Watt, J.T., Johnson, S.Y., Langenheim, V.E., Scheirer, D.S., Rosenberg, L.I., Graymer, R.W., and Kvitek, R., 2009, Geologic mapping in the Central California coastal zone: integrating geology, geophysics, and geomorphology: Geological Society of America Abstracts with Programs, v. 41, n. 7, p. 283.

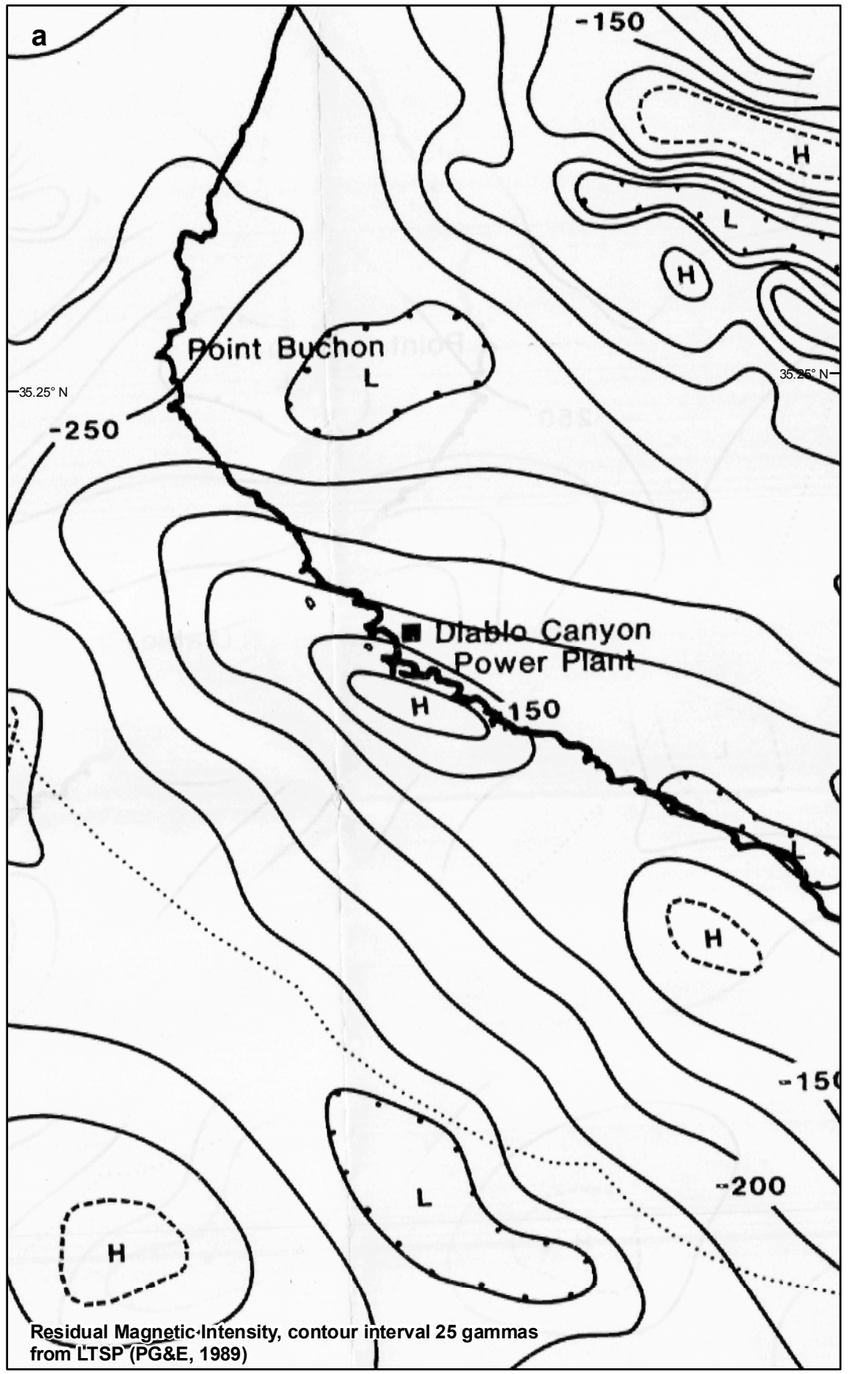

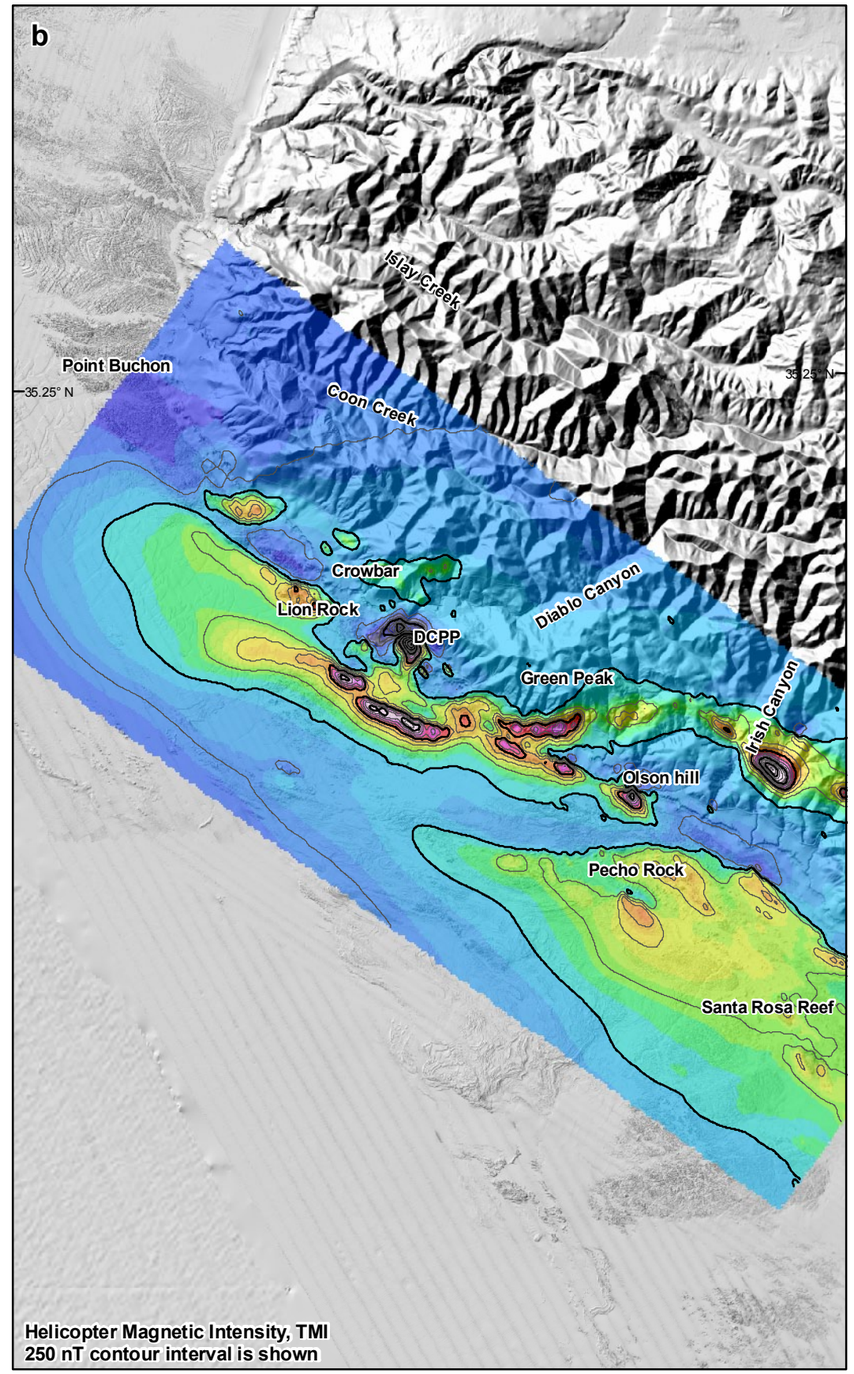

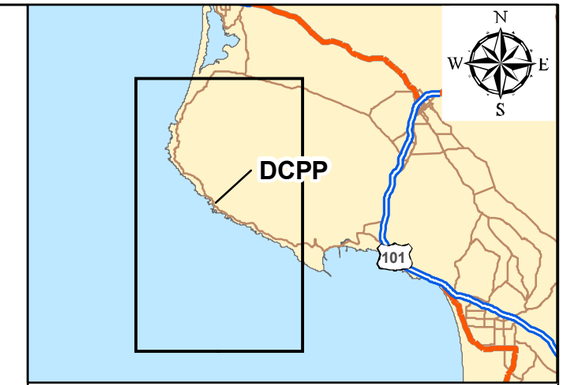

LEGEND

Total Magnetic Intensity
(nanoteslas)

- > 48,160
- 48,100
- 48,000
- 47,900
- 47,800
- 47,700
- < 47660

Map scale: 1:100,000
Map projection: NAD 1983, UTM Zone 10 North

0 1 2 Miles
0 2 4 Kilometers

Comparison of 1989 LTSP Residual Magnetic Intensity with 2009 Helicopter Total Magnetic Intensity anomaly map

SHORELINE FAULT STUDY **12/01/2010**

Pacific Gas and Electric Company | Figure **D-1**

File path: S:\13800\13838\13838.002\Figures\20101112_Report\Appendix_D\Figure_D-1.mxd; Date: [12/1/2010]; User: S. Bozkurt

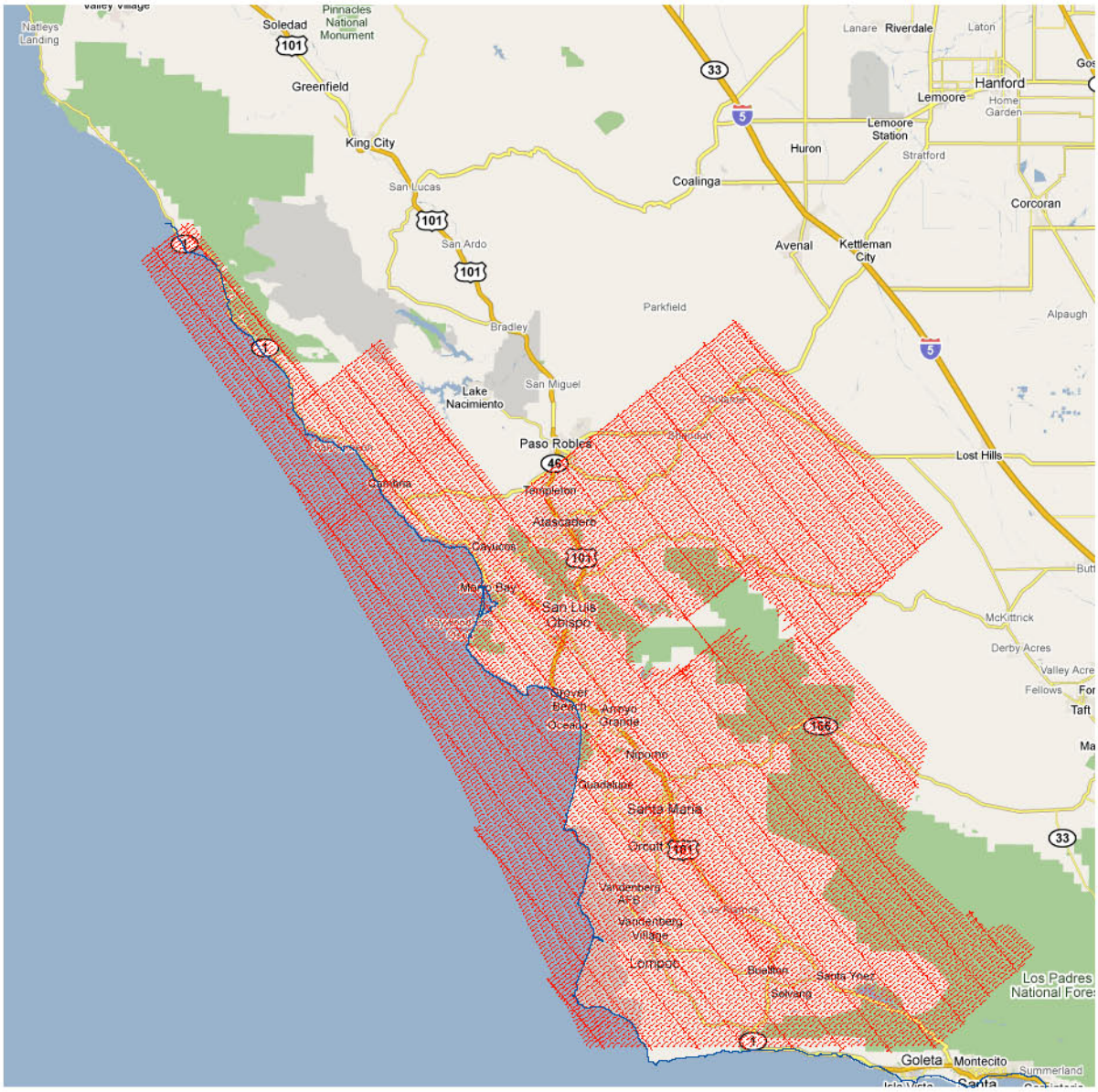

2008 aeromagnetic survey tracklines along the central California Coast Ranges (Langenheim et al., 2009)

SHORELINE FAULT STUDY	11/22/2010
Pacific Gas and Electric Company	Figure D-2

File path: S:\13800\13838\13838.002\Figures\20101112_Report\Appendix_D\Figure_D-2.mxd; Date: [11/22/2010]; User: S. Bozkurt

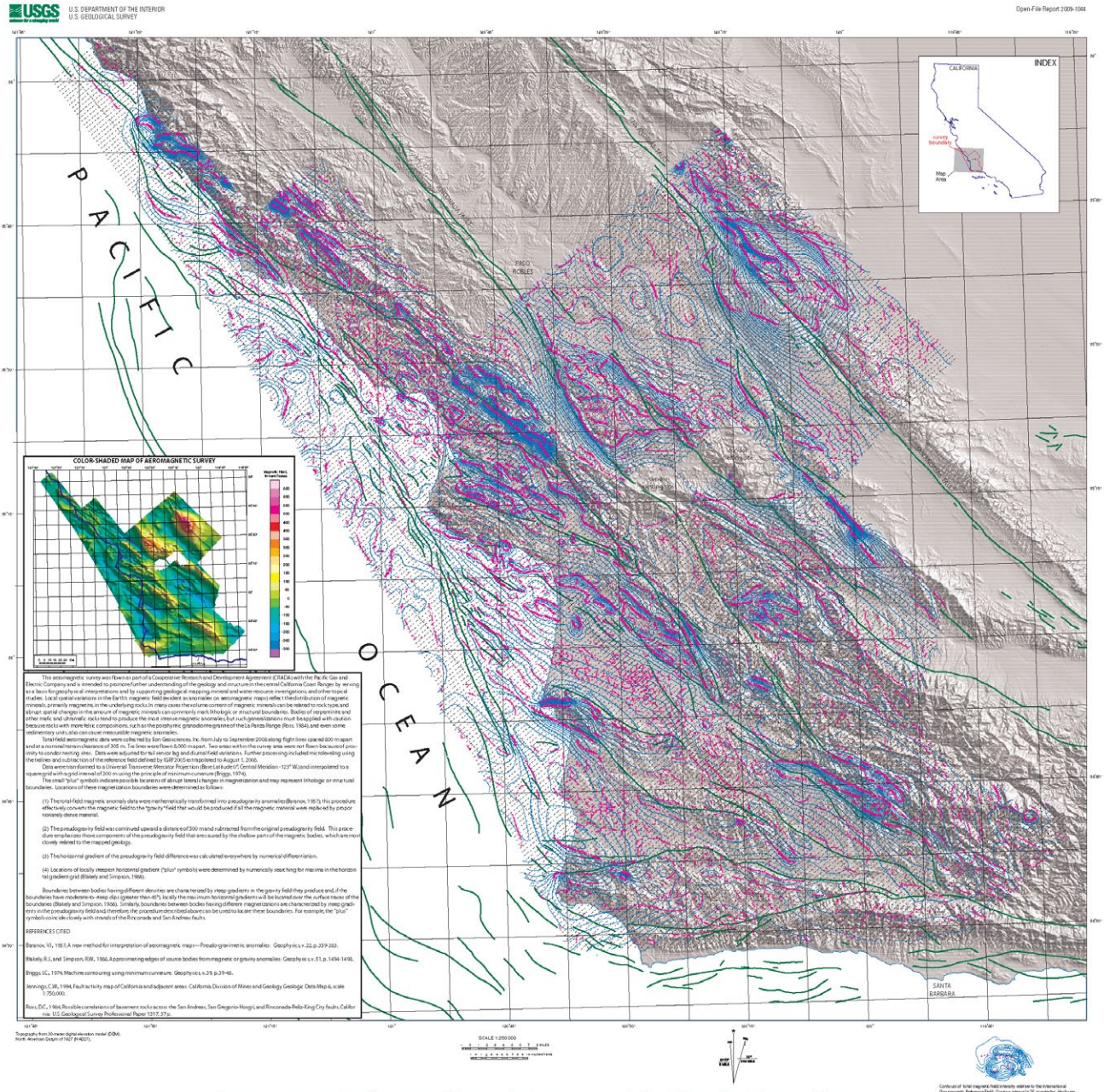

Aeromagnetic survey map of the central California Coast Ranges (Langenheim et al., 2009)

SHORELINE FAULT STUDY	11/22/2010
Pacific Gas and Electric Company	Figure D-3

File path: S:\13800\13838\13838.002\Figures\20101112_Report\Appendix_D\Figure_D-3.mxd; Date: [11/22/2010]; User: S. Bozkurt

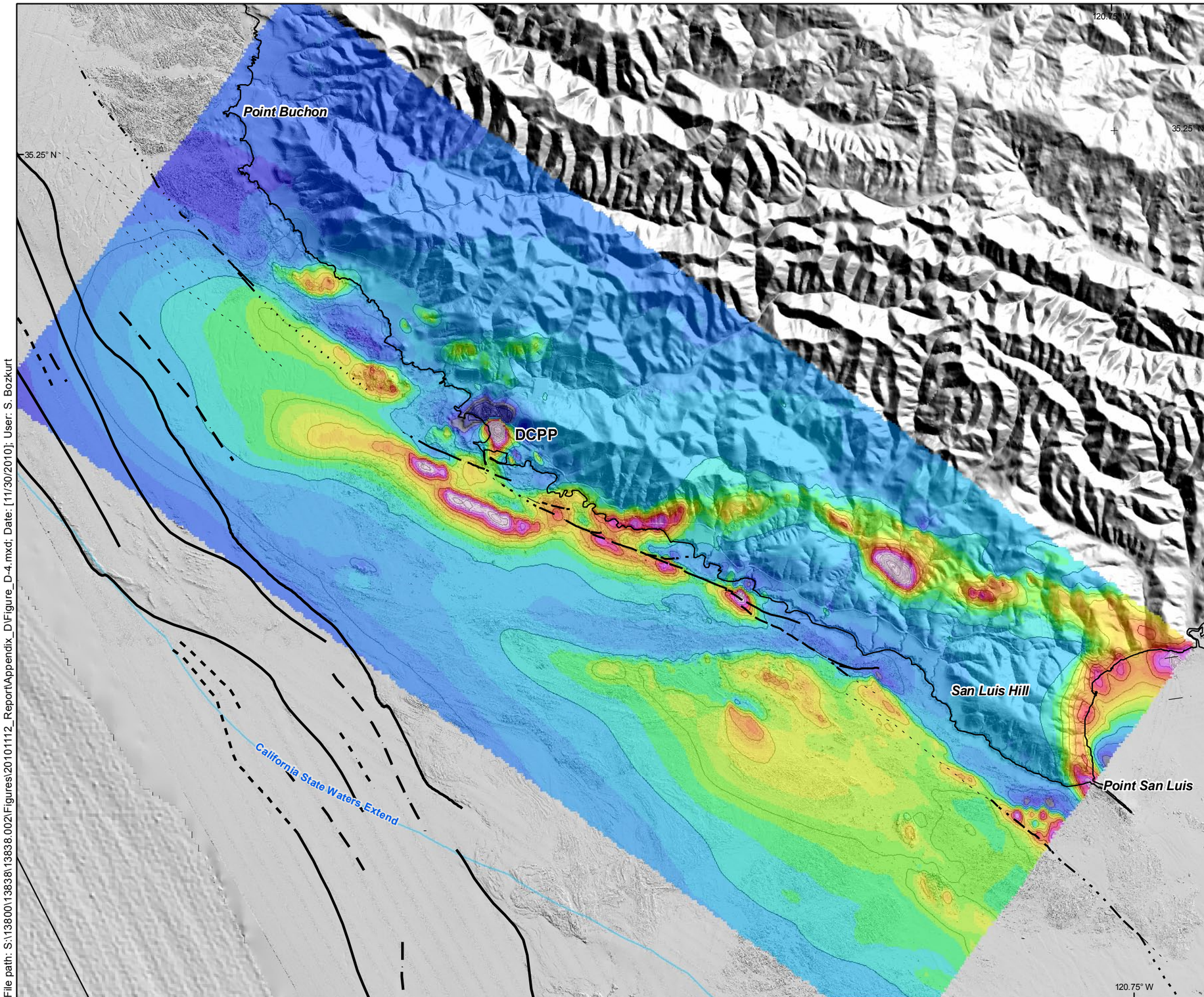

LEGEND

Total Magnetic Intensity (nanoteslas)

- < 47660
- 47,700
- 47,800
- 47,900
- 48,000
- 48,100
- > 48,160

Map scale: 1:60,000
Map projection: NAD 1983, UTM Zone 10 North

0 1 2 Miles

0 1 2 Kilometers

Total Magnetic Intensity map for the 2009 Helicopter Survey Area

SHORELINE FAULT STUDY **11/30/2010**

Pacific Gas and Electric Company | Figure **D-4**

File path: S:\13800\13838\13838.002\Figures\20101112_Report\Appendix_D\Figure_D-4.mxd; Date: [11/30/2010]; User: S. Bozkurt

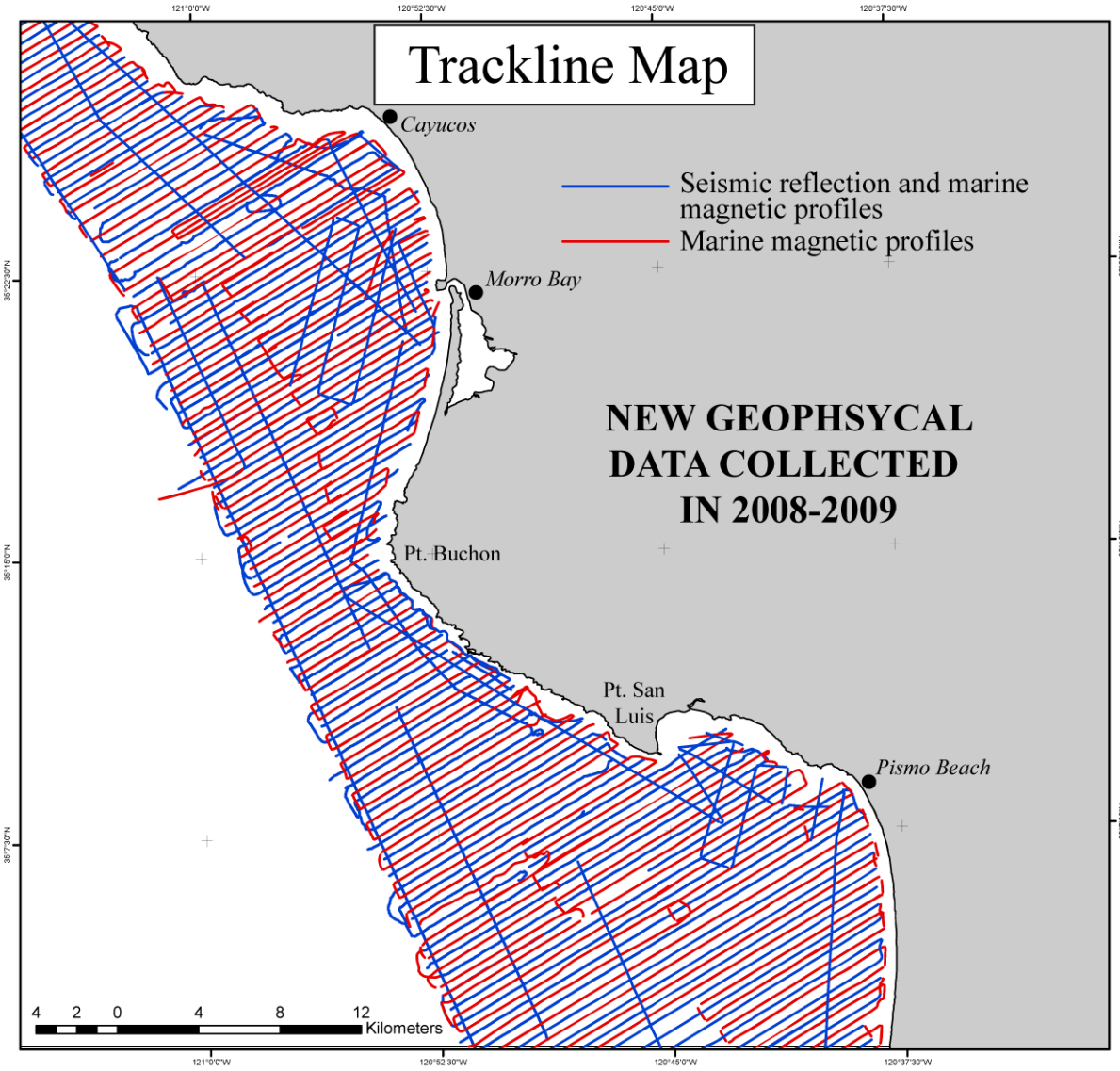

Notes: Blue lines represent ship tracks where high resolution marine seismic reflection and magnetic data were collected at 800 m spacing. Red lines are additional marine magnetics ship tracks for a net 400 m spacing (Watt et al., 2009).

Track line map of marine geophysical data collected in 2008 and 2009.

SHORELINE FAULT STUDY	**11/22/2010**
Pacific Gas and Electric Company	Figure **D-5**

File path: S:\13800\13838\13838.002\Figures\20101112_Report\Appendix_D\Figure_D-3.mxd; Date: [11/22/2010]; User: S. Bozkurt

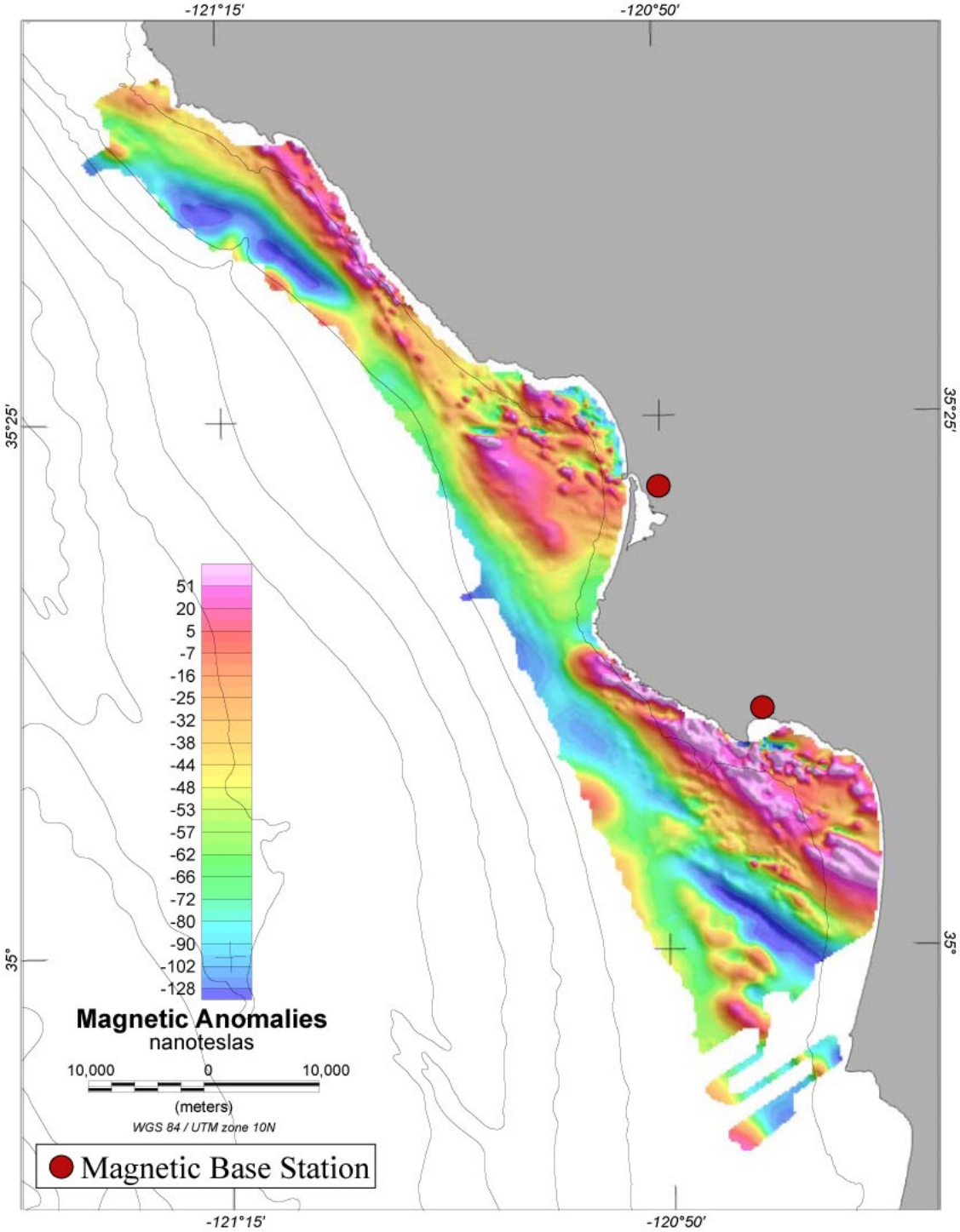

Magnetic anomaly map of the 2008-2009 marine survey area (Sliter et al., 2009)

SHORELINE FAULT STUDY	**11/22/2010**
Pacific Gas and Electric Company	Figure **D-6**

File path: S:\13800\13838\13838.002\Figures\20101112_Report\Appendix_D\Figure_D-6.ai; Date: [11/22/2010]; User: S. Bozkurt

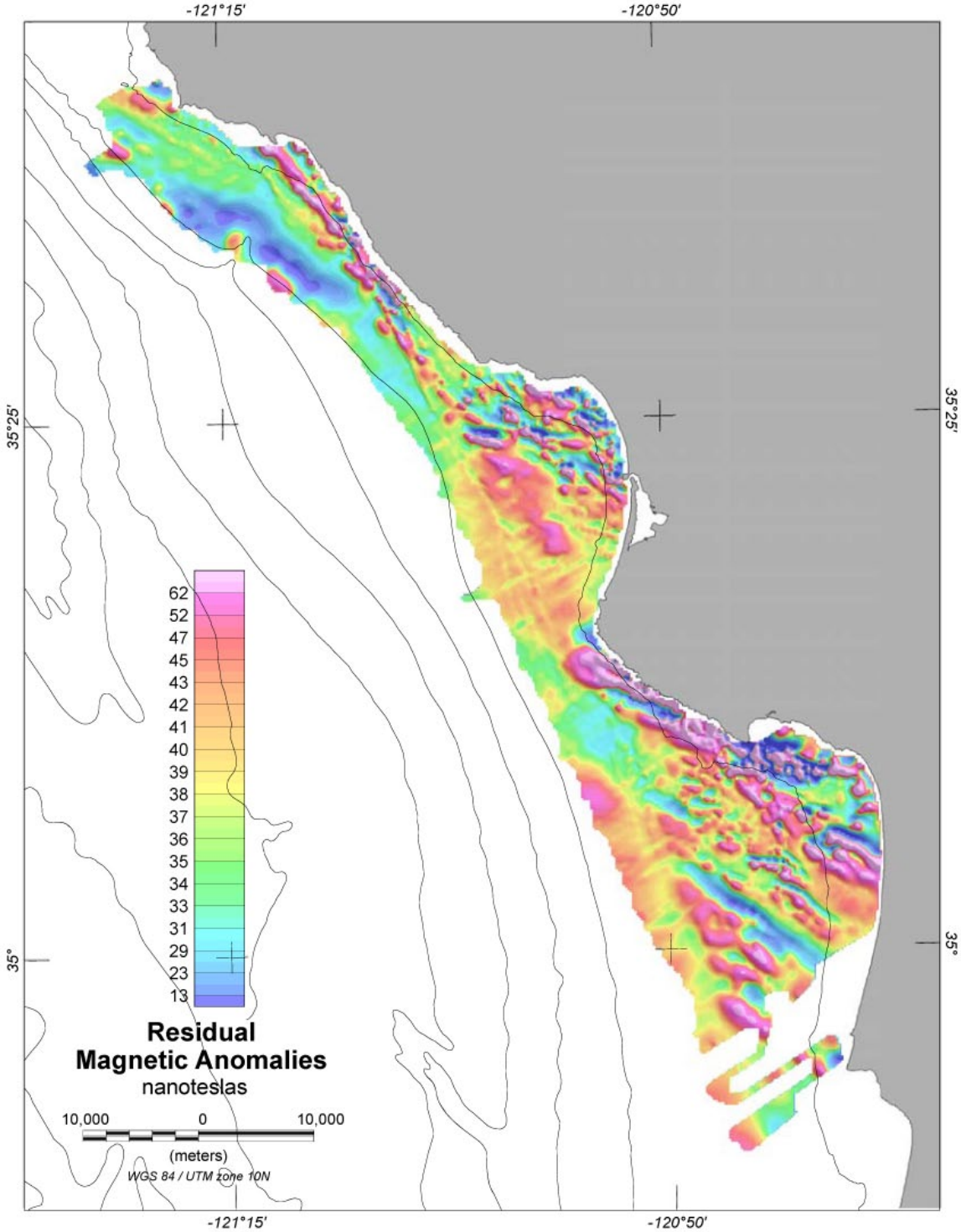

Residual magnetic anomaly map of the shallow subsurface (< 500 m) in the 2008/2009 marine survey area (Sliter et al., 2009)

SHORELINE FAULT STUDY	11/22/2010
Pacific Gas and Electric Company	Figure D-7

File path: S:\13800\13838\13838.002\Figures\20101112_Report\Appendix_D\Figure_D-7.ai; Date: [11/22/2010]; User: S. Bozkurt

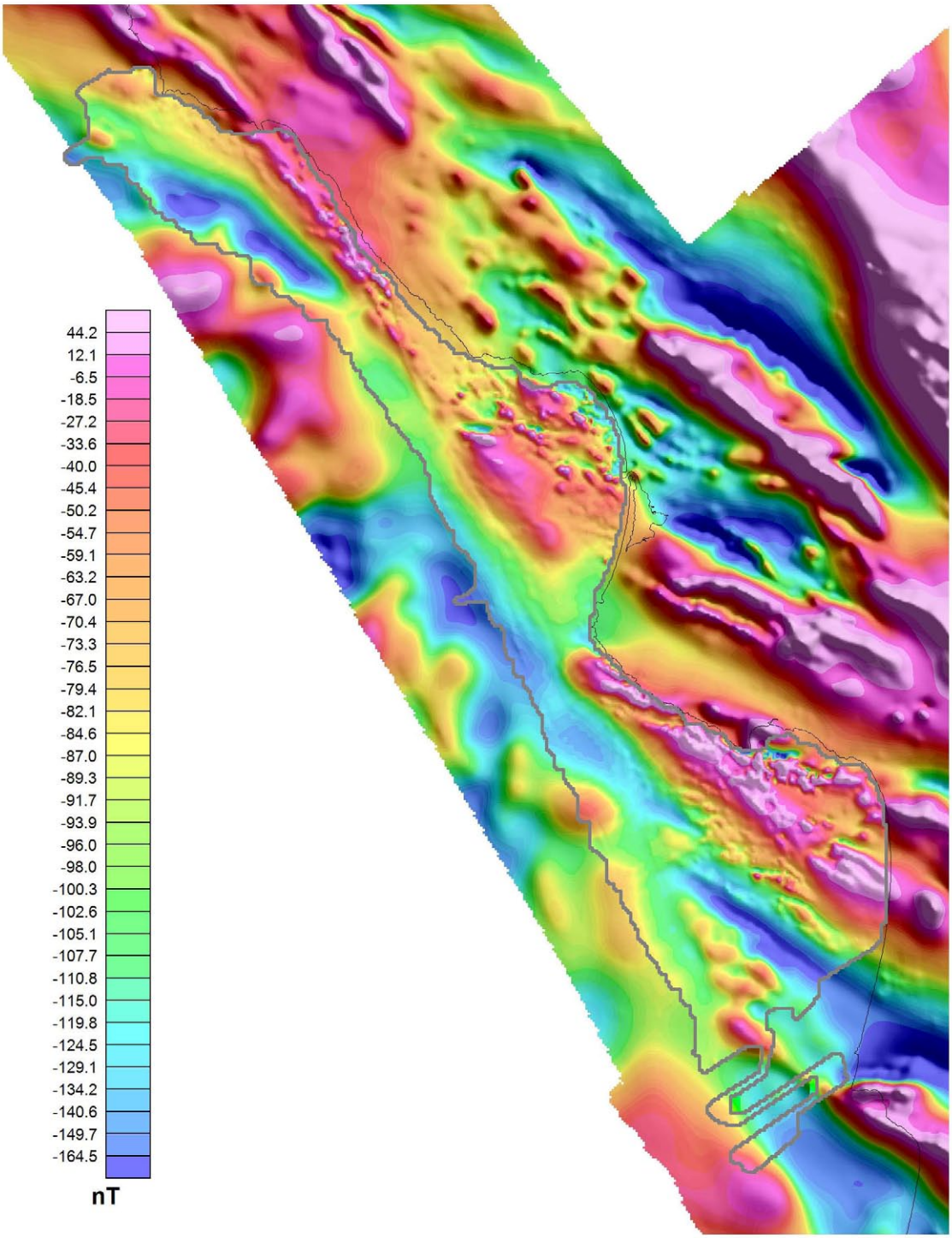

Notes: Marine magnetic data were filtered to effectively place those data at the same height as the aeromagnetic data (~ 305 m) (Langenheim et al., 2009)

Merged aeromagnetic and marine magnetics data

SHORELINE FAULT STUDY **11/22/2010**

Pacific Gas and Electric Company

Figure **D-8**

File path: S:\13800\13838\13838.002\Figures\20101112_Report\Appendix_D\Figure_D-8.ai; Date: [11/22/2010]; User: S. Bozkurt

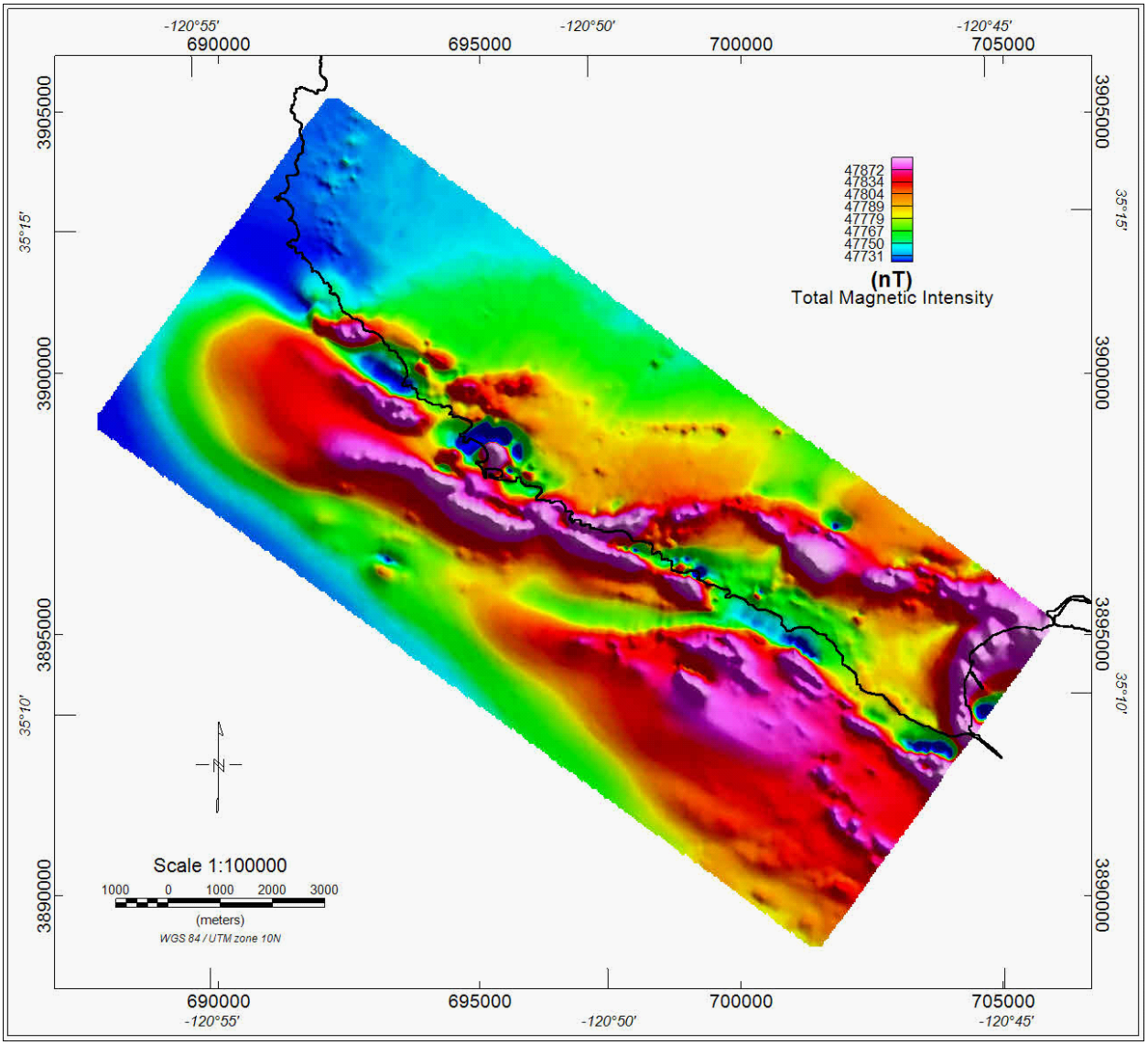

Helicopter total magnetic intensity re-gridded to 30 m spacing

SHORELINE FAULT STUDY	11/22/2010
Pacific Gas and Electric Company	Figure D-9

File path: S:\13800\13838\13838.002\Figures\20101112_Report\Appendix_D\Figure_D-9.ai; Date: [11/22/2010]; User: S. Bozkurt

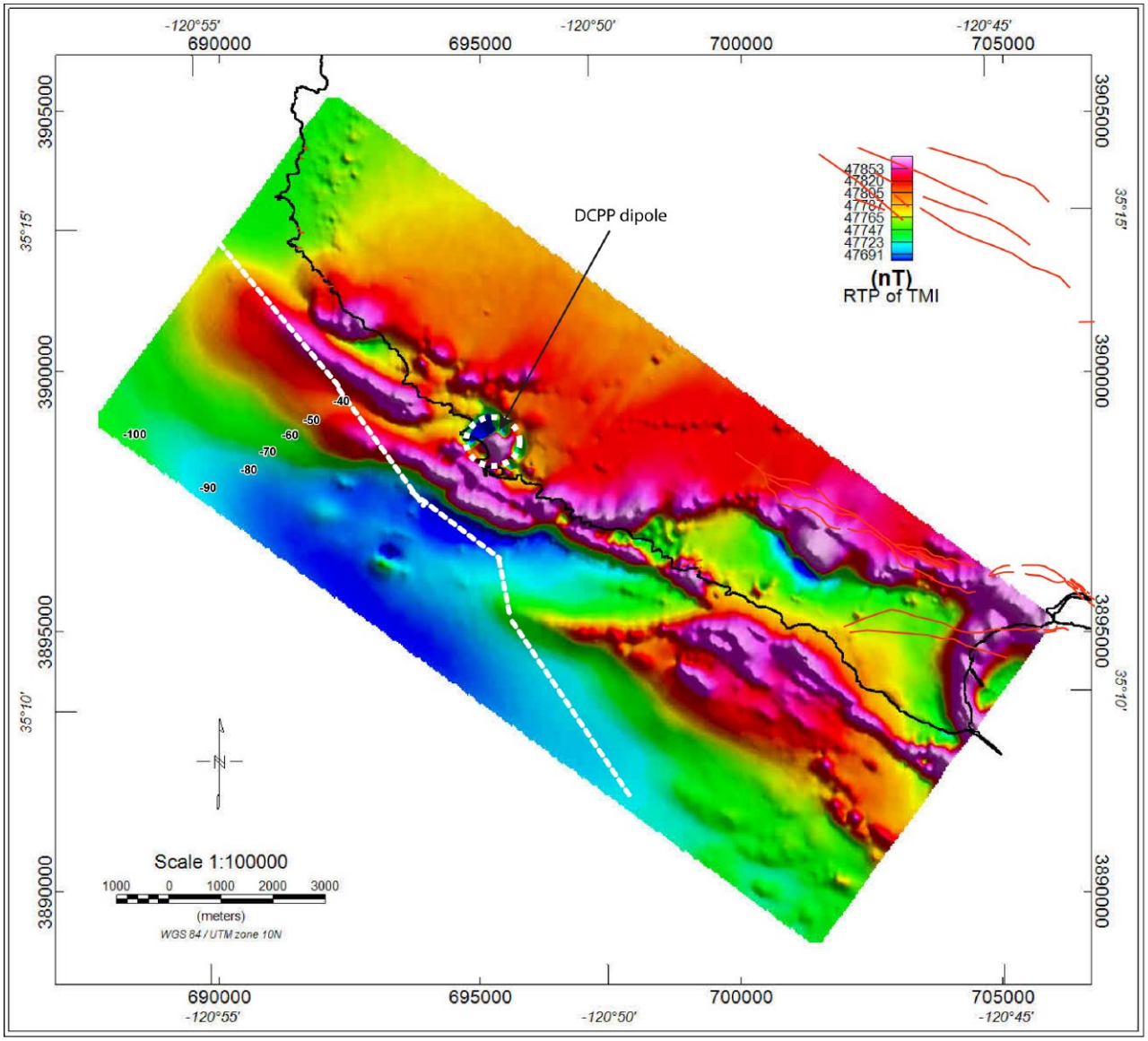

Note: The approximate region of water depths of 40 m or more is southwest of the short-dashed white line

Reduction to Pole Transformation of the Total Magnetic Intensity Map

SHORELINE FAULT STUDY **11/30/2010**

Pacific Gas and Electric Company

Figure **D-10**

File path: S:\13800\13838\13838.002\Figures\20101112_Report\Appendix_D\Figure_D-10.ai; Date: [11/22/2010]; ser: S. Bozkurt

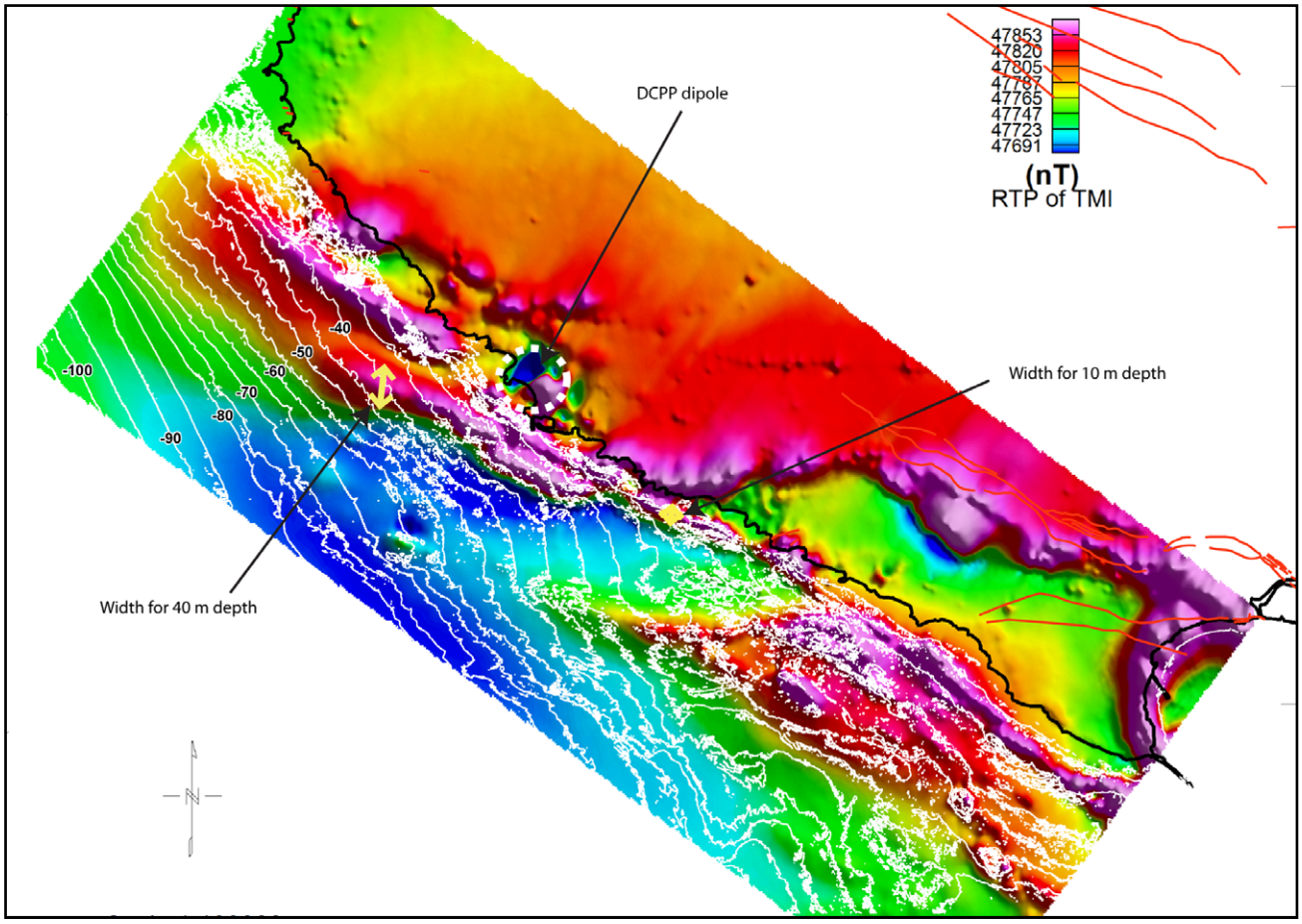

Notes: The yellow double-arrow on the -40 m contour illustrates that the Shoreline fault anomaly width is about three times wider in the region of 40 m water depth than the anomaly width in 10 m of water near the shore (smaller yellow double arrow as indicated). The white dashed circle outlines the region dominated by the dipole response to the DCPP.

Bathymetry in m (negative to denote depth below sea level) as white contours on the RTP field map

SHORELINE FAULT STUDY	**11/22/2010**
Pacific Gas and Electric Company	Figure **D-11**

File path: S:\13800\13838\13838.002\Figures\20101112_Report\Appendix_D\Figure_D-11.ai; Date: [11/22/2010]; ser: S. Bozkurt

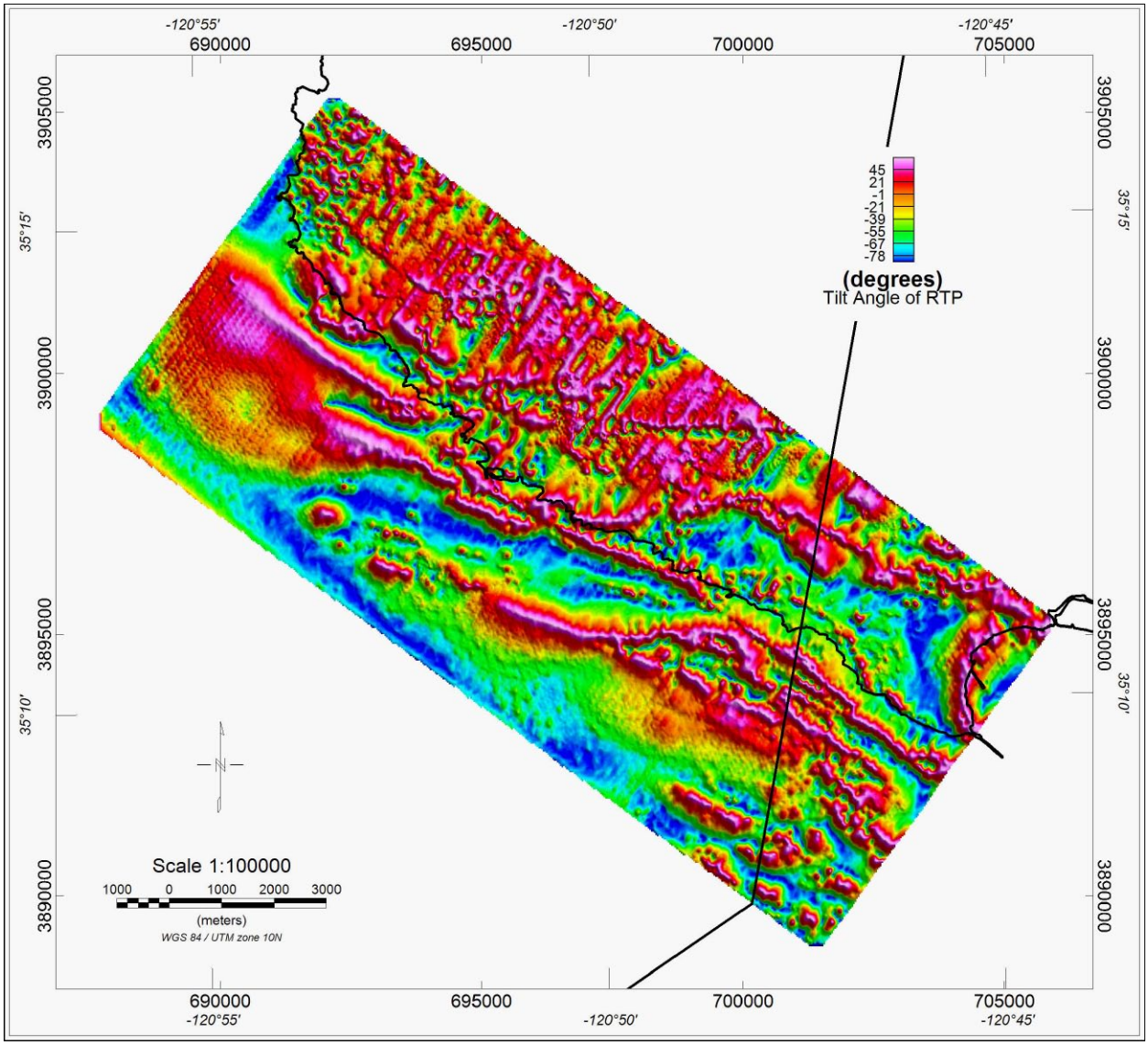

Tilt Angle Magnetic Anaomaly Map based on 2009 Helicopter RTP Anomaly Map

SHORELINE FAULT STUDY	**11/30/2010**
Pacific Gas and Electric Company	Figure **D-12**

File path: S:\13800\13838\13838.002\Figures\20101112_Report\Appendix_D\Figure_D-12.ai; Date: [11/22/2010]; ser: S. Bozkurt

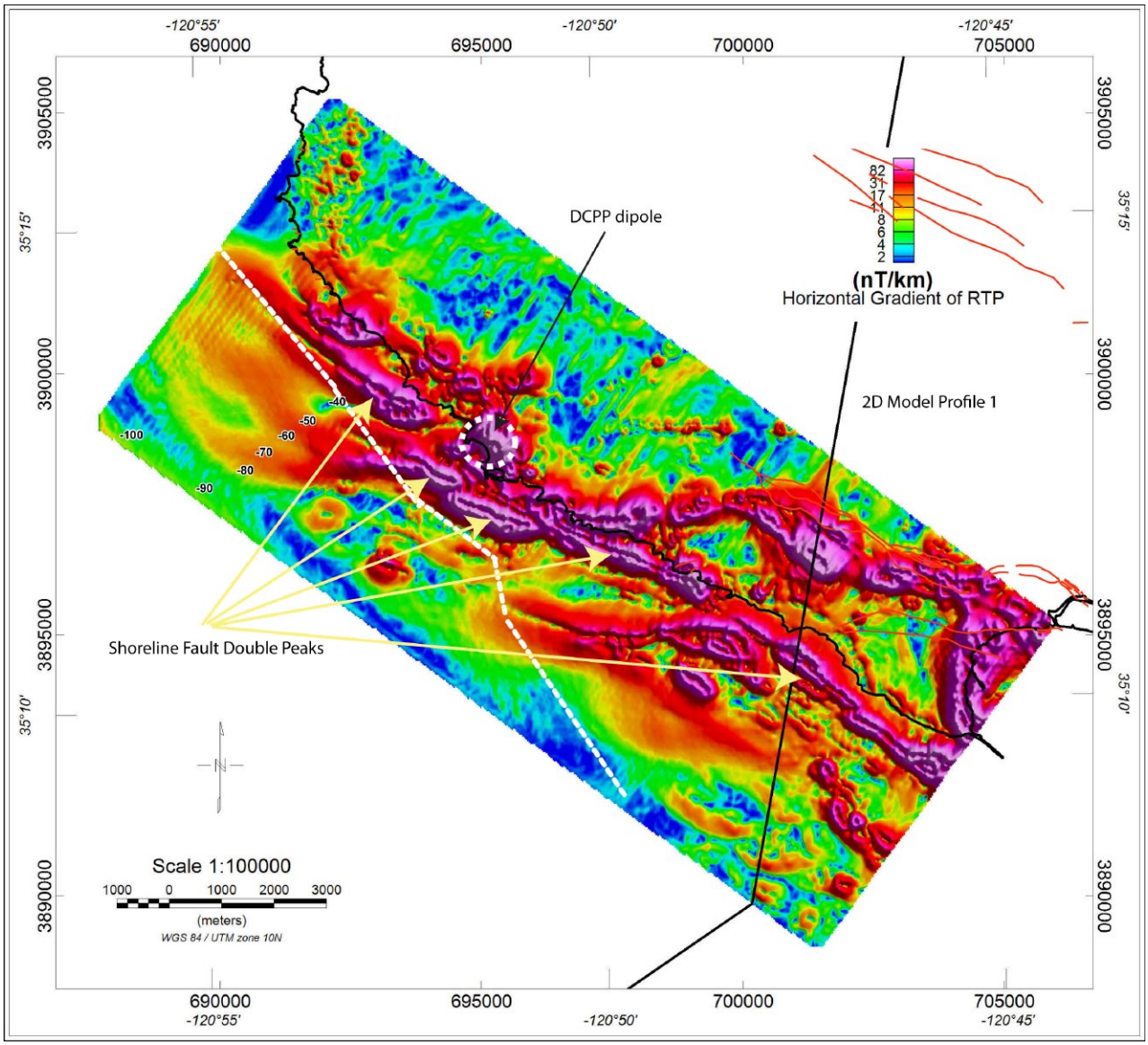

Notes: The approximate region of water depths of 40 m or more is southwest of the short-dashed white line

Horizontal Gradient of Helicopter Reduction to Pole Anomaly Map

SHORELINE FAULT STUDY	**11/30/2010**
Pacific Gas and Electric Company	Figure **D-13**

File path: S:\13800\13838\13838.002\Figures\20101112_Report\Appendix_D\Figure_D-13.ai; Date: [11/22/2010]; ser: S. Bozkurt

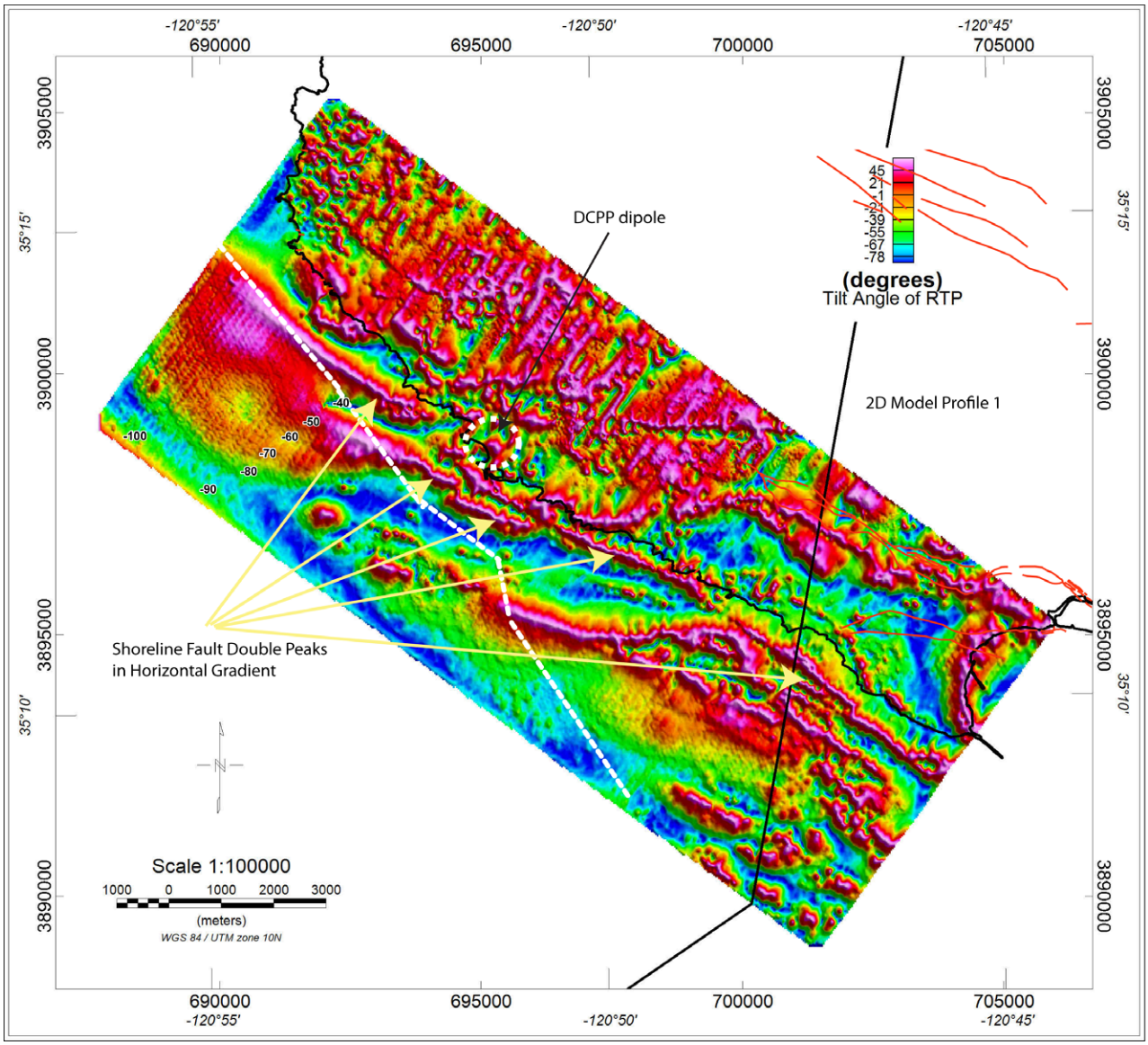

Notes: 40 m bathymetry contour in meters as the short-dashed white line separating deeper water to the southwest from shallower water to the northeast.

Tilt angle of the helicopter RTP with the approximate 40 m bathymetry contour

SHORELINE FAULT STUDY	**11/22/2010**
Pacific Gas and Electric Company	Figure **D-14**

File path: S:\13800\13838\13838.002\Figures\20101112_Report\Appendix_D\Figure_D-14.ai; Date: [11/22/2010]; ser: S. Bozkurt

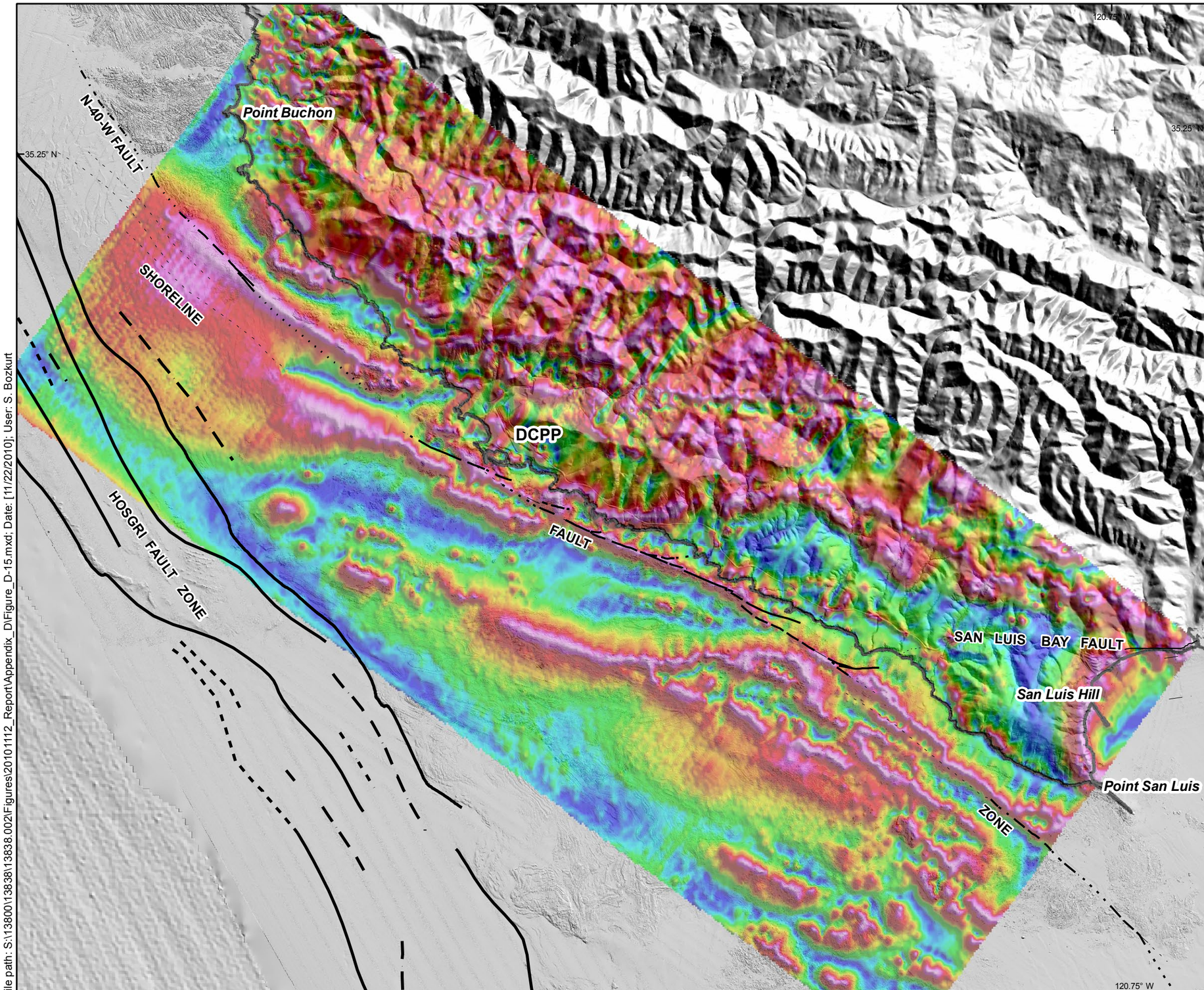

LEGEND

Offshore faults from this study (2010)

45
21
-1
-21
-39
-55
-67
-78

2010 Helicopter Magnetic Anomaly Survey

Tilt angle of RTP is shown in degrees

Map scale: 1:60,000
Map projection: NAD 1983, UTM Zone 10 North

0 1 2 Miles

0 1 2 Kilometers

Tilt-angle of RTP superimposed on terrain with offshore faults

SHORELINE FAULT STUDY **11/22/2010**

Pacific Gas and Electric Company

Figure **D-15**

File path: S:\13800\13838\13838.002\Figures\20101112_Report\Appendix_D\Figure_D-15.mxd; Date: [11/22/2010]; User: S. Bozkurt

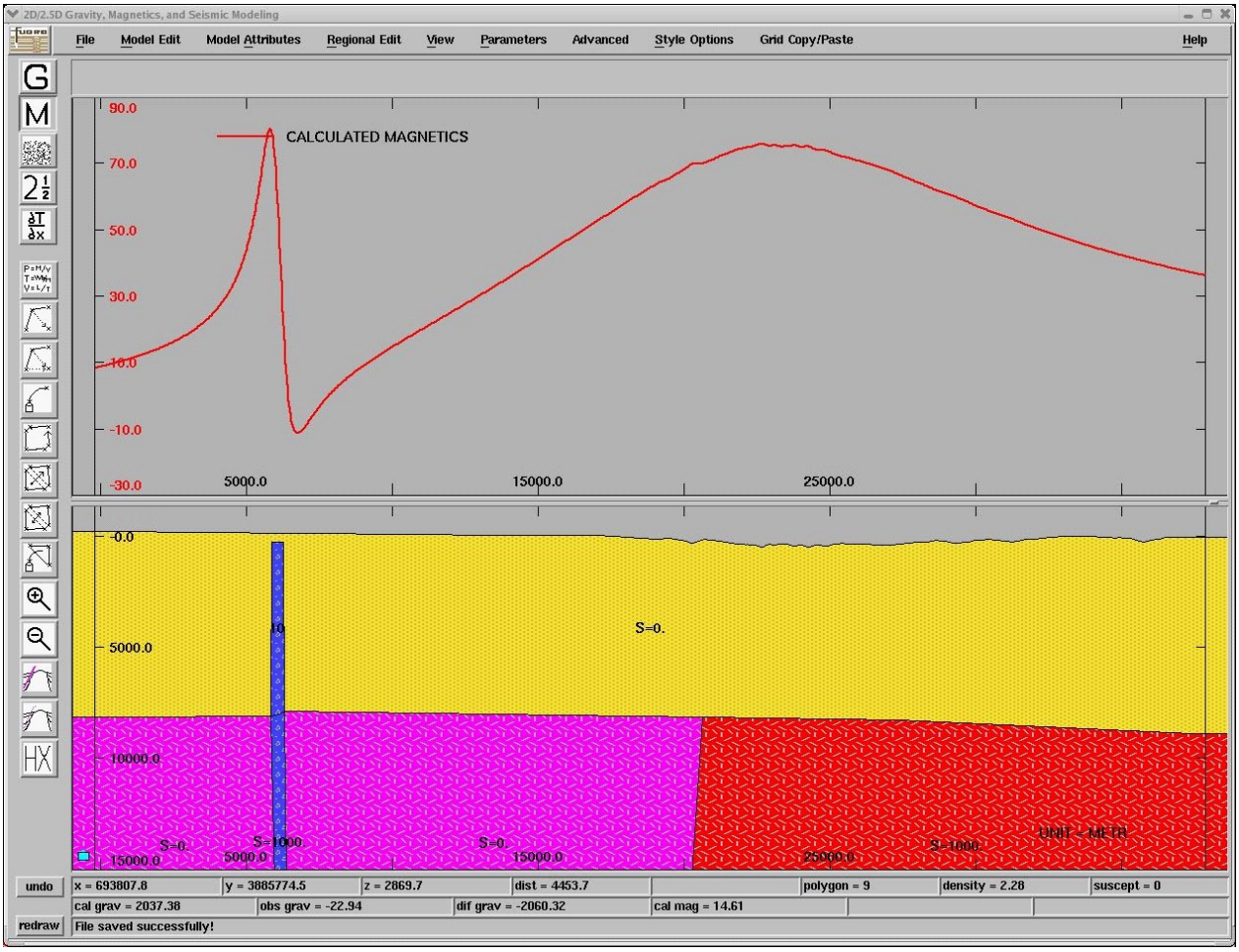

Test magnetic model with line azimuth of 008º

SHORELINE FAULT STUDY	**11/22/2010**
Pacific Gas and Electric Company	Figure **D-16**

File path: S:\13800\13838\13838.002\Figures\20101112_Report\Appendix_D\Figure_D-16.ai; Date: [11/22/2010]; ser: S. Bozkurt

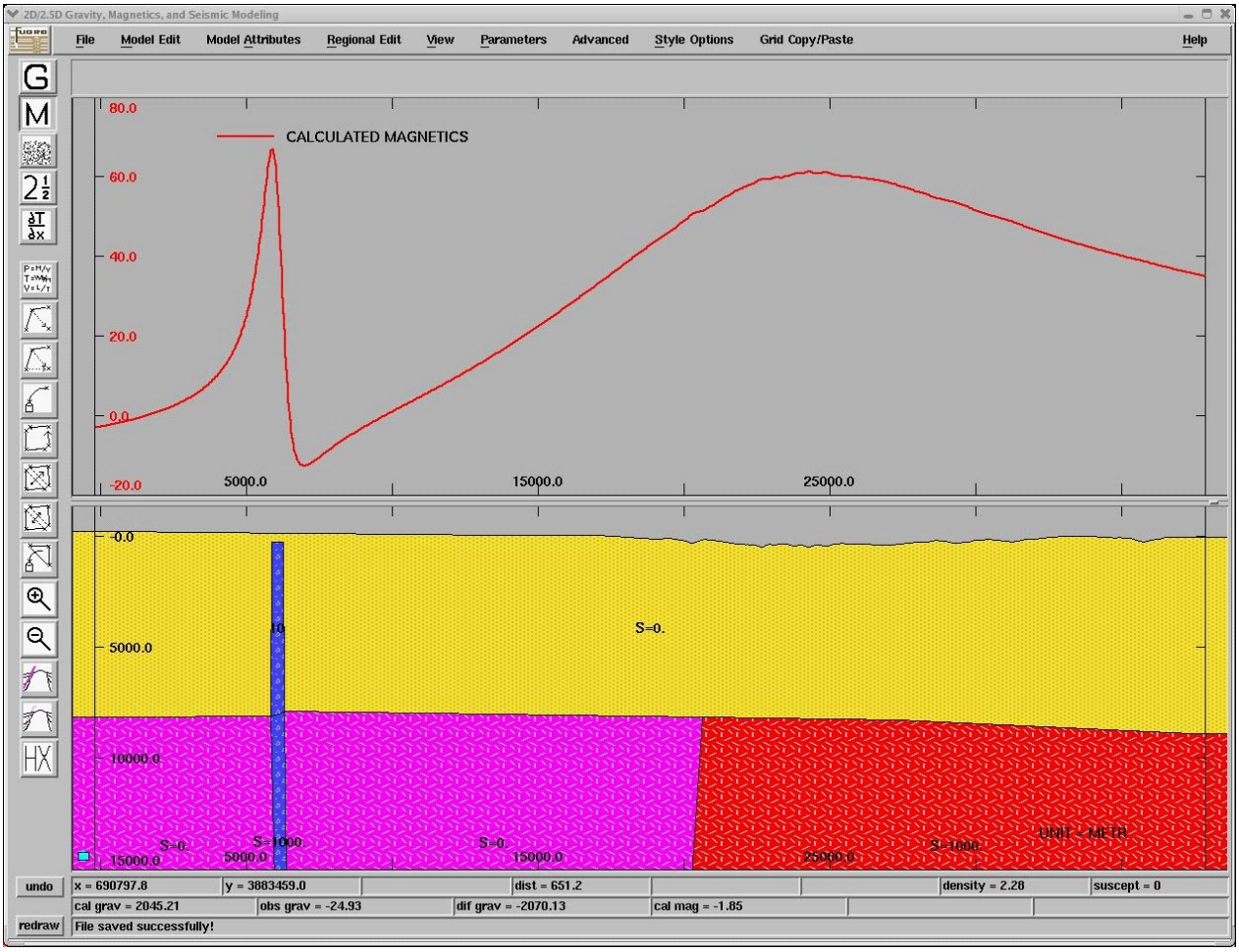

Test magnetic model with line azimuth of 058º

SHORELINE FAULT STUDY	**11/22/2010**
Pacific Gas and Electric Company	Figure **D-17**

File path: S:\13800\13838\13838.002\Figures\20101112_Report\Appendix_D\Figure_D-17.ai; Date: [11/22/2010]; ser: S. Bozkurt

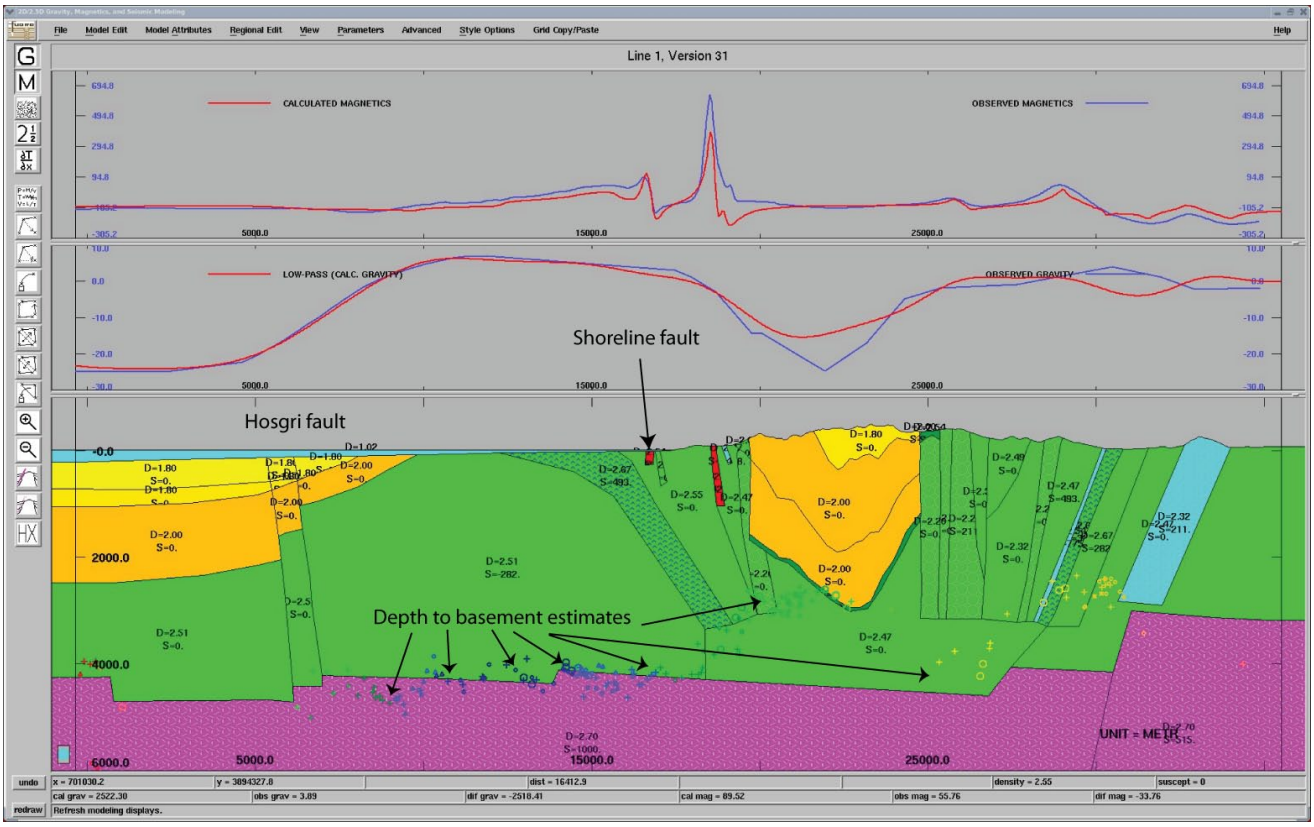

Notes: Forward modeling magnetic (top) and gravity (middle) anomaly fits (red curves) to observed data (blue curves) using the density and magnetic susceptibility model (bottom) consistent with first-order geologic and geophysical constraints

Forward Modeling of Magnetic and Gravity Data

SHORELINE FAULT STUDY	**11/30/2010**
Pacific Gas and Electric Company	Figure **D-18**

File path: S:\13800\13838\13838.002\Figures\20101112_Report\Appendix_D\Figure_D-18.ai; Date: [11/22/2010]; ser: S. Bozkurt

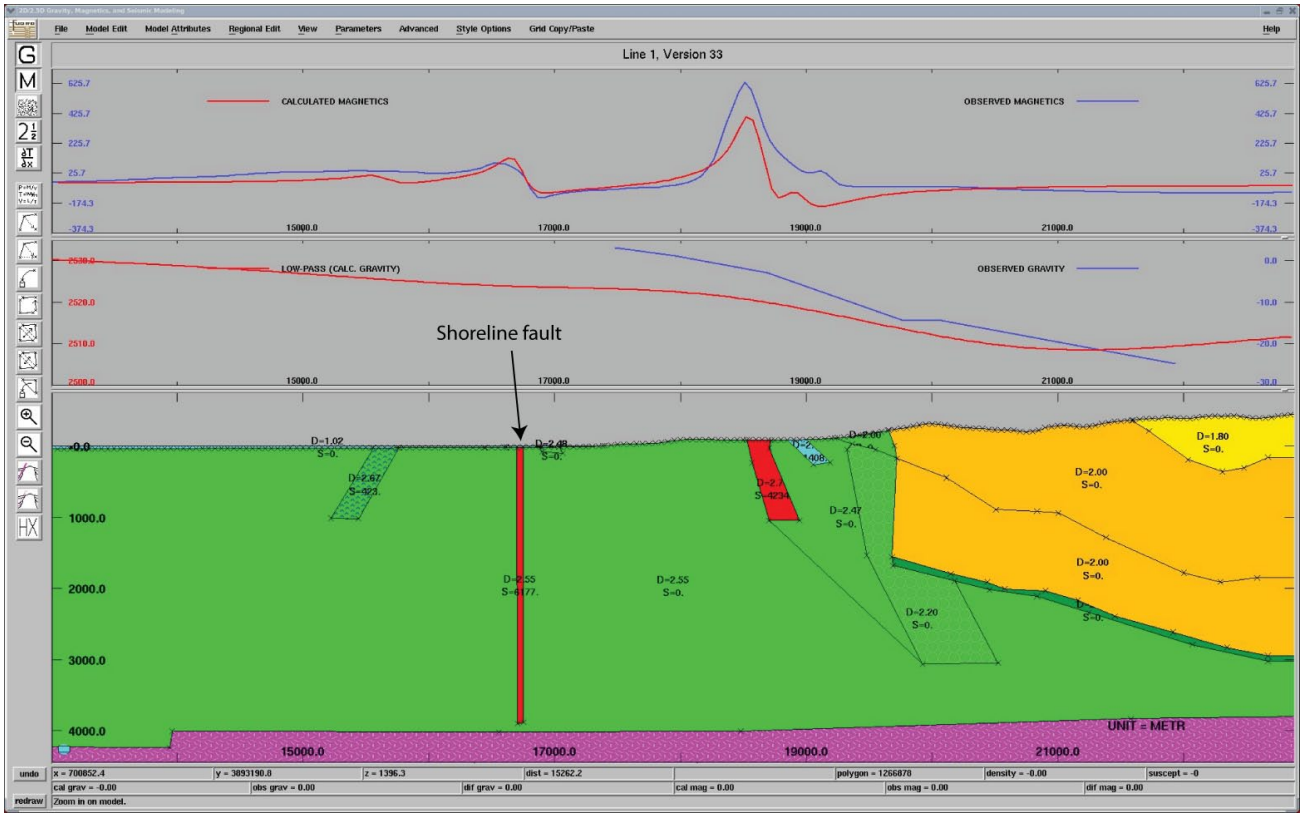

Magnetic sensitivity test with a thin, vertical Shoreline fault magnetic body (model 33)

SHORELINE FAULT STUDY	11/22/2010
Pacific Gas and Electric Company	Figure D-19

File path: S:\13800\13838\13838.002\Figures\20101112_Report\Appendix_D\Figure_D-19.ai; Date: [11/22/2010]; ser: S. Bozkurt

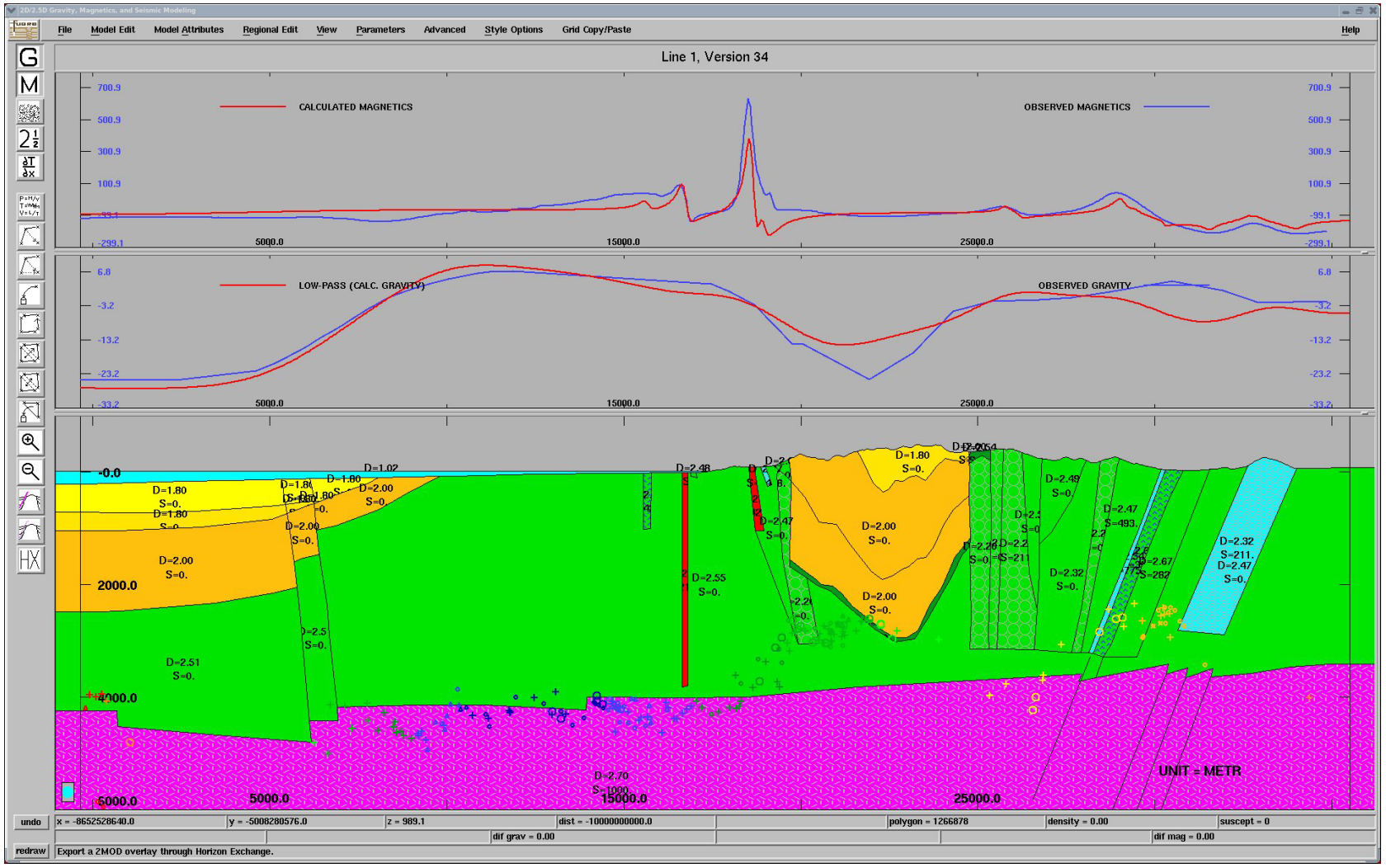

Magnetic sensitivity test with a 200-m-thick vertical Shoreline fault magnetic body (model 34)

SHORELINE FAULT ZONE STUDY

Pacific Gas and Electric Company

Figure D - 20a

File path: S:\13800\13838\13838.002\Figures\20101112_Report\stu\Figure_1.ai; Date: [12/20/2010]; User: S. Bozkurt

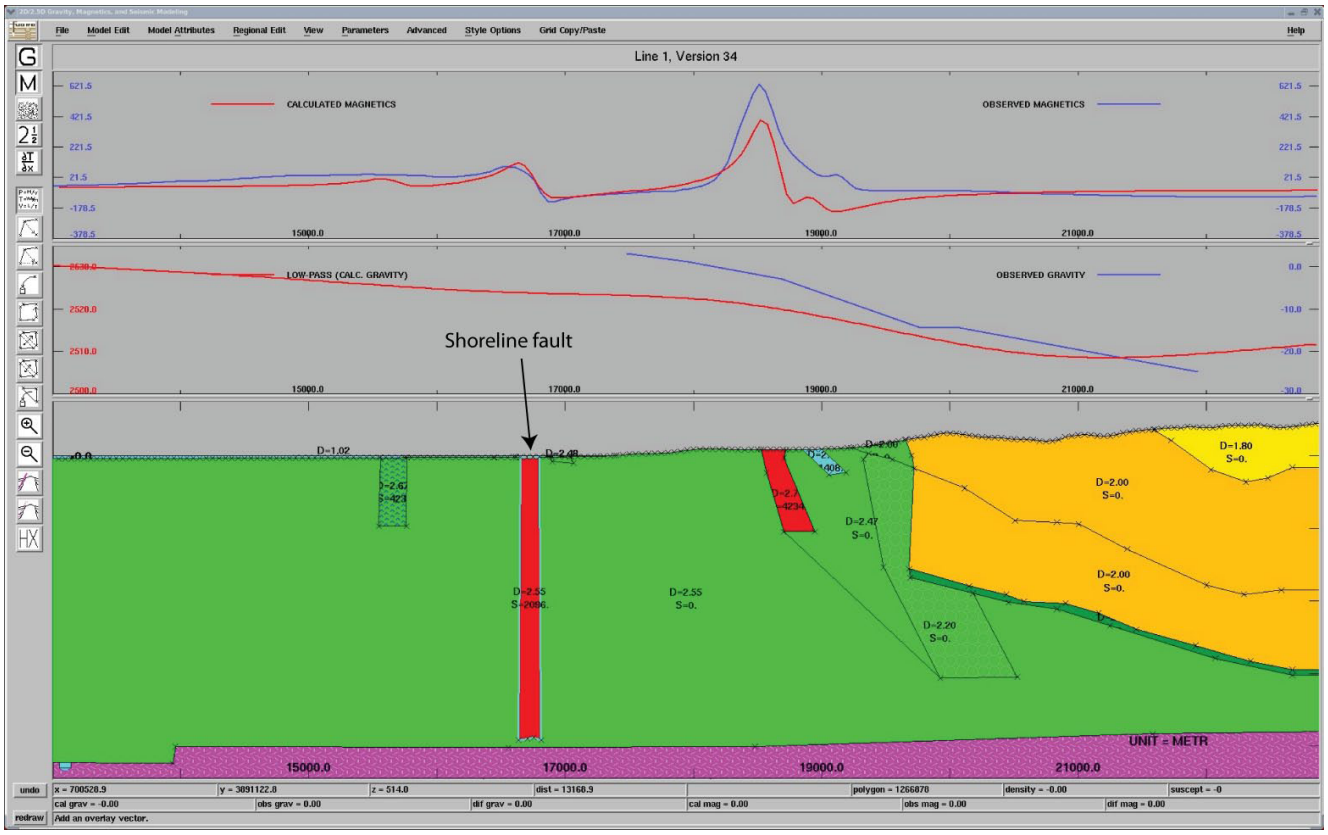

Magnetic sensitivity test with a 200-m-thick vertical Shoreline fault magnetic body (model 34)

SHORELINE FAULT STUDY

Pacific Gas and Electric Company

Figure D - 20b

File path: S:\13800\13838\13838.002\Figures\20101112_Report\Appendix_D\Figure_D-20.ai; Date: [11/22/2010]; ser: S. Bozkurt

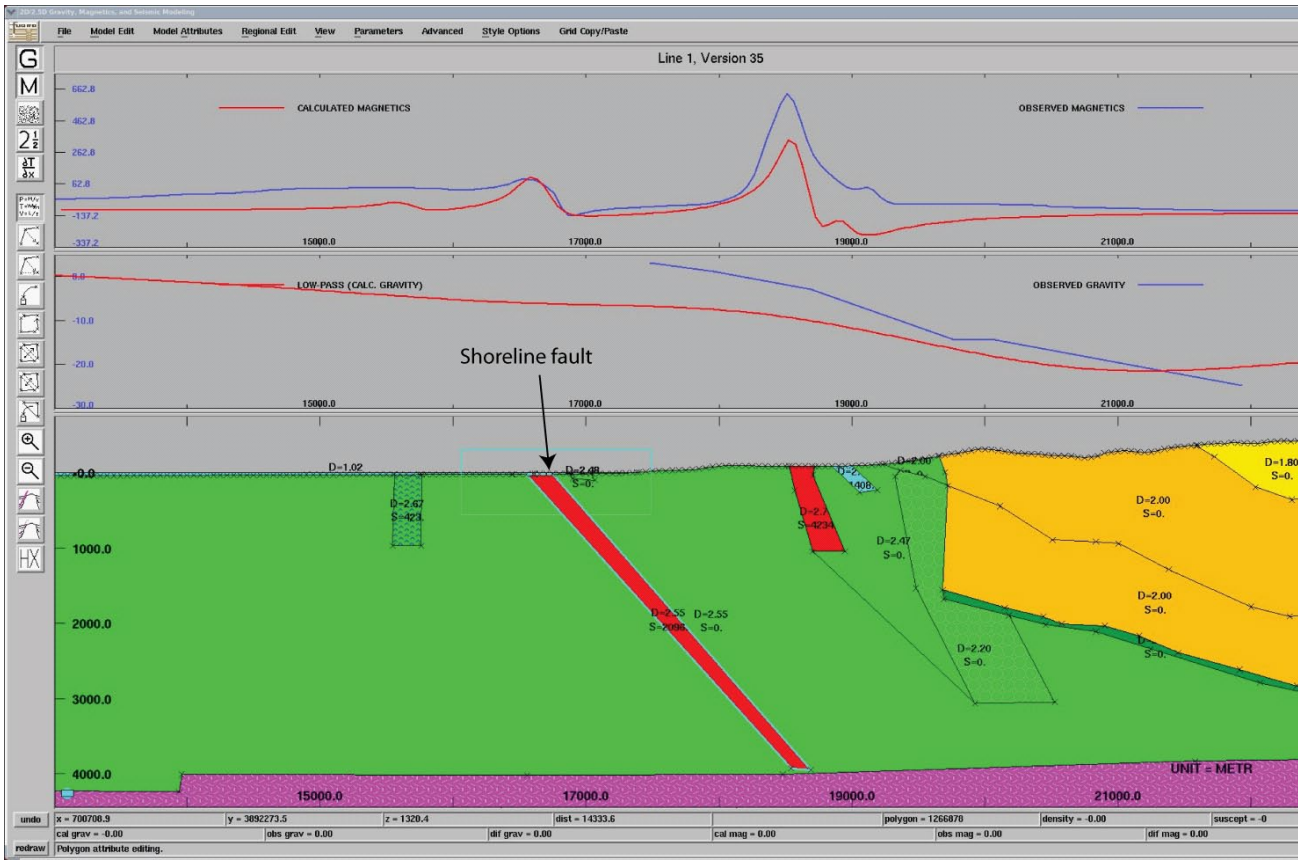

Magnetic sensitivity test with a 200-m-thick north-dipping Shoreline fault magnetic body (model 35)

SHORELINE FAULT STUDY	11/22/2010
Pacific Gas and Electric Company	Figure **D-21**

File path: S:\13800\13838\13838.002\Figures\20101112_Report\Appendix_D\Figure_D-21.ai; Date: [11/22/2010]; ser: S. Bozkurt

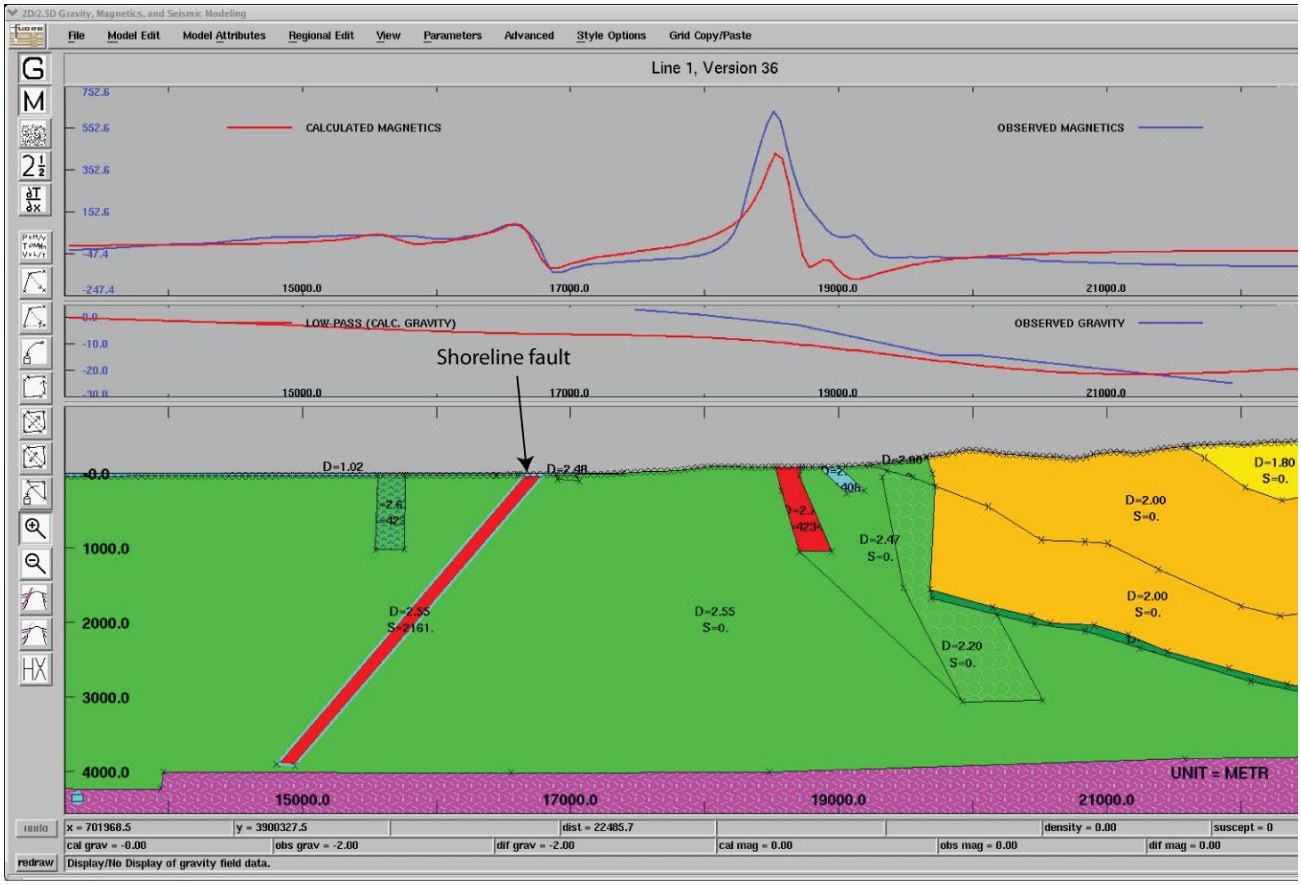

Magnetic sensitivity test with a 200-m-thick south-dipping Shoreline fault magnetic body (model 36)

SHORELINE FAULT STUDY	11/22/2010
Pacific Gas and Electric Company	Figure **D-22**

File path: S:\13800\13838\13838.002\Figures\20101112_Report\Appendix_D\Figure_D-22.ai; Date: [11/22/2010]; ser: S. Bozkurt